

THE ROBUSTNESS OF DARK MATTER DENSITY PROFILES IN DISSIPATIONLESS MERGERS

STELIOS KAZANTZIDIS,^{1,2} ANDREW R. ZENTNER,² AND ANDREY V. KRAVTSOV^{2,3}
*The *Astrophysical Journal*, submitted*

ABSTRACT

We present a comprehensive series of dissipationless N -body simulations to investigate the evolution of density distribution in equal-mass mergers between dark matter (DM) halos and multicomponent galaxies. The DM halo models are constructed with various asymptotic power-law indices ranging from steep cusps to core-like profiles and the structural properties of the galaxy models are motivated by the Λ CDM paradigm of structure formation. The adopted force resolution allows robust density profile estimates in the inner $\sim 1\%$ of the virial radii of the simulated systems. We demonstrate that the central slopes and overall shapes of the remnant density profiles are virtually identical to those of the initial systems suggesting that the remnants retain a remarkable memory of the density structure of their progenitors, despite the relaxation that accompanies merger activity. We also find that halo concentrations remain approximately constant through hierarchical merging involving identical systems and show that remnants contain significant fractions of their bound mass well beyond their formal virial radii. These conclusions hold for a wide variety of initial asymptotic density slopes, orbital energies, and encounter configurations, including sequences of consecutive merger events, simultaneous mergers of several systems, and mergers of halos with embedded cold baryonic components in the form of disks, spheroids, or both. As an immediate consequence, the net effect of gas cooling, which contracts and steepens the inner density profiles of DM halos, should be preserved through a period of dissipationless major merging. Our results imply that the characteristic universal shape of DM density profiles may be set early in the evolution of halos.

Subject headings: cosmology: theory — dark matter — galaxies: halos — halos: structure — halos: density profiles — methods: numerical

1. INTRODUCTION

In the currently favored cold dark matter (CDM) paradigm of hierarchical structure formation (e.g., Blumenthal et al. 1984), galaxy assembly initiates with the gravitational collapse of overdense regions into halos of dark matter (DM), the average density of which exceeds that of baryonic matter by roughly six to one (e.g., Spergel et al. 2003). Bound in the potential wells of DM halos, baryons cool, condense, and form galaxies with a variety of properties (e.g., White & Rees 1978; Blumenthal et al. 1984). Understanding the nonlinear gravitational collapse of the DM is the necessary first step in gaining insight into the physical processes of galaxy formation.

During the past decade the mass distribution of virialized DM halos has been the subject of extensive numerical investigations (e.g., Dubinski & Carlberg 1991; Navarro et al. 1996, hereafter NFW; Fukushige & Makino 1997; Moore et al. 1999, hereafter M99; Klypin et al. 2001; Fukushige & Makino 2001; Power et al. 2003; Tasitsiomi et al. 2004; Diemand et al. 2004; Fukushige et al. 2004). These studies have established that the spherically-averaged density profiles of CDM halos can be described by an approximately “universal” formula

over the entire range of mass and length scales that these simulations can resolve. This universal density profile is comprised of an inner steep cusp with $\rho(r) \propto r^{-\gamma}$, where $1 \lesssim \gamma \lesssim 1.5$, and a power-law decline $\rho(r) \propto r^{-3}$ in the outer parts. The origin of this simple form of the density distribution is not yet understood, but it has been conjectured that merging should play a noteworthy role in determining DM halo profiles (e.g., Wechsler et al. 2002; Zhao et al. 2003; Loeb & Peebles 2003; Lu et al. 2005).

Numerous authors have considered the effect of mergers on the evolution of the density distribution of halos using controlled numerical experiments (e.g., White 1978; Farouki et al. 1983; Villumsen 1983; Syer & White 1998; Barnes 1999; Fulton & Barnes 2001; Boylan-Kolchin & Ma 2004; Moore et al. 2004; Aceves & Velazquez 2005). These studies employed collisionless N -body merger simulations and reached the conclusion that the density structure of the merger remnants is reminiscent of that of their progenitors. However, most of these investigations used idealized, non-rotating, spherical systems to represent the halo and galaxy models and were restricted to a narrow range of encounter orbital energies. Furthermore, the great majority of these earlier studies did not explore the effect of hierarchical merging on the evolution of the DM distribution and with the notable exception of Aceves & Velazquez (2005), did not address the role of a baryonic component and internal angular momentum in shaping the inner density profiles of merger remnants. Yet, the gravitational field in the central regions of galaxies is dominated by baryons and, in the standard paradigm of structure formation, galaxies and galaxy halos in the universe are the end result of a complex hierarchy of mergers. Elucidating the effect

¹ Institute for Theoretical Physics, University of Zürich, Winterthurerstrasse 190, CH-8057 Zürich, Switzerland; stelios@physik.unizh.ch.

² Kavli Institute for Cosmological Physics and Department of Astronomy and Astrophysics, The University of Chicago, 5640 South Ellis Avenue, Chicago, IL 60637 USA; zentner@kicp.uchicago.edu, andrey@oddjob.uchicago.edu.

³ The Enrico Fermi Institute, 5640 South Ellis Ave., The University of Chicago, Chicago, IL 60637 USA.

of internal angular momentum on the evolution of halo density profiles is fundamental as previous studies have already indicated (e.g., Bullock et al. 2001a; Ascasibar et al. 2004).

Despite the inexorable increase in the dynamic range of current numerical simulations, several important issues remain unresolved. For example, radiative cooling and condensation of baryons in the halo centers, which is a precursor of galaxy formation, steepens the density distribution of DM (Zeldovich et al. 1980; Barnes & White 1984; Blumenthal et al. 1986; Ryden & Gunn 1987; Gnedin et al. 2004). It is essential to ascertain whether late mergers, that take place after the majority of baryonic cooling has occurred, can modify the net effect of dissipation on halo density profiles, as conjectured by Loeb & Peebles (2003) and Gao et al. (2004). In addition, it is worth asking if the density distributions of halos today are related to the density profiles of their progenitors and whether halos retain any memory of earlier epochs, as is expected from analytical considerations (e.g., Mathur 1988; Dehnen 2005). Addressing these questions may aid in understanding the dependence of halo concentration on halo mass (Navarro et al. 1997; Bullock et al. 2001b; Eke et al. 2001) and its relation to halo mass-accretion-rates and formation times (Wechsler et al. 2002; Zhao et al. 2003).

The complexity of halo formation in a cosmological context, with continuous mergers, accretion, and rapidly changing potential wells, hinders isolation of the mechanisms that drive the evolution of halo density profiles. We have therefore decided to examine the evolution of density structure in *controlled* mergers of DM halos and multicomponent galaxies using a large ensemble of dissipationless *N*-body simulations. We improve upon the work of previous authors by adopting self-consistent realizations for the DM halo models and employing realistic models for the progenitor galaxies motivated by the prevailing Λ CDM paradigm of structure formation. Our simulation set is carefully designed to allow an investigation of a much larger parameter space than before and our primary goal is to establish conclusively the degree to which the density profiles of remnants retain memory of the structures of their progenitors over a wide range of inner density slopes, internal and orbital angular momenta, and in the presence of cold baryonic components.

We conduct numerical experiments that extend and expand upon those of earlier studies in at least two important aspects. For the first time, we perform a thorough study of the effect of a merger sequence on the density profile of DM halos in an attempt to mimic the hierarchical mass assembly that characterizes CDM-like cosmological models. Moreover, the impact of a stellar component on the density distribution of DM during mergers has not been addressed to date with detailed simulations of realistic progenitor galaxy models. As we illustrate below, the central density slopes of the merging systems are notably robust and the overall shapes of remnant density profiles are related to a remarkable degree to those of their progenitors. Our results firmly establish that equal-mass mergers will not suffice to modify the central density slopes and overall shape profiles of the DM distribution.

The outline of this paper is as follows. In Section 2, we present the halo and galaxy models used in this study

and the numerical methods we employ to construct them. We also describe in detail our simulation techniques and conduct convergence tests and numerical relaxation experiments that illustrate the robustness of our results to numerical effects. Section 3 contains results of the analysis applied to binary and multiple mergers of halos and multicomponent galaxies. Implications and extensions of these findings are discussed in Section 4. Finally, in Section 5, we summarize our main results.

2. NUMERICAL METHODS

2.1. Halo Models

We consider DM halo models with density profiles that are described by the general form (Zhao 1996; Kravtsov et al. 1998),

$$\rho(r) = \frac{\rho_s}{(r/r_s)^\gamma [1 + (r/r_s)^\alpha]^{(\beta-\gamma)/\alpha}} \quad (r \leq r_{\text{vir}}), \quad (1)$$

where γ is the *asymptotic* inner slope of the profile, β is the outer slope, and α parametrizes the transition between the inner and outer profiles, with larger values of α corresponding to sharper transitions. Here, ρ_s is a characteristic inner density and r_s denotes the scale radius defined as the distance from the center where the logarithmic slope is the average of the inner and outer slopes, $d \ln \rho(r) / d \ln r = -(\gamma + \beta)/2$. The logarithmic slope corresponding to the density profile of equation (1) is given by

$$\frac{d \ln \rho(r)}{d \ln r} = -\gamma - (\beta - \gamma) \frac{(r/r_s)^\alpha}{[1 + (r/r_s)^\alpha]}. \quad (2)$$

It is worth emphasizing that the choice of the functional form of the halo profiles is not unique. Several recent numerical studies have suggested that the density distributions of DM halos are better represented by a function with a logarithmic slope continuously varying as a power law in radius (Stoehr et al. 2002; Navarro et al. 2004; Merritt et al. 2005; Graham et al. 2005). However, the adopted profiles constitute a sufficiently realistic representation of the density distribution of cosmological halos for the purposes of this study.

We define the virial radius, r_{vir} , as the radius enclosing an average density equal to the virial overdensity, Δ_{vir} , times the critical density for a flat universe, ρ_{crit} . Thus, the virial mass and virial radius are related through $M_{\text{vir}} = (4/3)\pi\rho_{\text{crit}}\Delta_{\text{vir}}r_{\text{vir}}^3$. Throughout the paper we adopt the concordance Λ CDM cosmological model ($\Omega_m = 0.3$, $\Omega_\Lambda = 0.7$, $h = 0.7$) and assume $z = 0$. The virial overdensity is then equal to $\Delta_{\text{vir}} \simeq 103.5$ (e.g., Lacey & Cole 1993; Eke et al. 1998). The general form of equation (1) includes as special cases many of the density profiles commonly used to fit DM halos in cosmological simulations. For example, the NFW and M99 density profiles correspond to the parameters $[\alpha, \beta, \gamma] = [1, 3, 1]$ and $[\alpha, \beta, \gamma] = [1.5, 3, 1.5]$, respectively.

One of the primary goals of this study is to examine the evolution of the inner density slopes during equal-mass dissipationless mergers. Hence, we fix the outer logarithmic slope to $\beta = -3$, as demonstrated by cosmological simulations (e.g., NFW; M99; Avila-Reese et al. 1999). However, density profiles with outer slopes $\beta \geq -3$ lead to cumulative mass profiles that diverge as $r \rightarrow \infty$. In order to keep the total mass finite, it is necessary to introduce a cutoff in the density profile. Truncating the

profile sharply for $r > r_{\text{vir}}$, results in unphysical models, therefore, we implement an exponential cutoff which sets in at the virial radius and turns off the profile on a scale r_{decay} . The truncation scale r_{decay} is a free parameter and controls the sharpness of the transition. Explicitly, we model the density profiles of halos beyond r_{vir} by

$$\rho(r) = \frac{\rho_s}{c(1+c)^2} \left(\frac{r}{r_{\text{vir}}} \right)^\kappa \exp \left[-\frac{r-r_{\text{vir}}}{r_{\text{decay}}} \right] (r > r_{\text{vir}}), \quad (3)$$

where $c \equiv r_{\text{vir}}/r_s$ is the concentration parameter. Finally, in order to ensure a smooth transition between the profile interior to r_{vir} given by equation (1) and the profile exterior to r_{vir} given by equation (3), we require the logarithmic slope to be continuous at $r = r_{\text{vir}}$. This implies

$$\kappa = \frac{-\gamma - \beta c^\alpha}{1 + c^\alpha} + \frac{r_{\text{vir}}}{r_{\text{decay}}}. \quad (4)$$

Note that this procedure results in some additional bound mass beyond r_{vir} , the precise amount of which depends upon the adopted model parameters. In the models we consider here, the mass exterior to r_{vir} is typically about $\sim 10\%$ of the mass contained within the virial radius.

We construct N -body halo models for this study using the method described in Kazantzidis et al. (2004b), which is based on an explicit computation of the exact phase-space distribution function (DF). Under the assumptions of spherical symmetry and an isotropic velocity dispersion tensor, the DF depends only on the binding energy per unit mass \mathcal{E} . In this case, the DF is given by

$$f(\mathcal{E}) = \frac{1}{\sqrt{8\pi^2}} \left[\int_0^{\mathcal{E}} \frac{d^2\rho}{d\psi^2} \frac{d\psi}{\sqrt{\mathcal{E}-\psi}} + \frac{1}{\sqrt{\mathcal{E}}} \left(\frac{d\rho}{d\psi} \right)_{\psi=0} \right] \quad (5)$$

(Eddington 1916), where $\rho(r)$ and $\psi(r)$ are the density profile and *relative* gravitational potential corresponding to the halo model, respectively. The second term on the right-hand side in equation (5) vanishes for any sensible behavior of $\psi(r)$ and $\rho(r)$ at large distances. The $d^2\rho/d\psi^2$ factor in the integrand would be difficult to deal with numerically, but it can be evaluated analytically using equations (1) and (3) for $\rho(r)$ to give an expression in which the only derivatives remaining are $d\psi/dr$ and $d^2\psi/dr^2$. Both of these can be written in terms of the density profile $\rho(r)$ and its cumulative mass distribution $M(r)$,

$$\frac{d^2\rho}{d\psi^2} = \left(\frac{r^2}{GM} \right)^2 \left[\frac{d^2\rho}{dr^2} + \frac{d\rho}{dr} \left(\frac{2}{r} - \frac{4\pi\rho r^2}{M} \right) \right]. \quad (6)$$

Thus, equation (5) is reduced to a simple quadrature with no numerical differentiation required which is integrated numerically to obtain the DF for the anticipated values of the energy \mathcal{E} . A Monte Carlo realization of the N -body model is then readily generated by randomly sampling the particle positions and velocities from the DF. This method makes no assumptions about the functional form of the local velocity distribution, and therefore produces self-consistent equilibria that are ideal for studies of the detailed structure of collisionless systems.

It is well established that cosmological halos exhibit departures from spherical symmetry and velocity isotropy

(e.g., Cole & Lacey 1996). Nevertheless, in § 3.2, we analyze merger simulations between systems resulting from binary encounters of the initial spherical and isotropic models. These merger remnants are known to reproduce the shape and velocity anisotropy trends found in cosmological simulations (Moore et al. 2004).

We model our halos with three density profiles specified by particular choices of the parameters in equation (1). The first model follows the NFW density profile with $[\alpha, \beta, \gamma] = [1, 3, 1]$, while the second and third models correspond to profiles with steeper ($[\alpha, \beta, \gamma] = [2, 3, 1.7]$) and shallower ($[\alpha, \beta, \gamma] = [2, 3, 0.2]$) inner slopes. In the interest of brevity, throughout the remainder of the text, we shall refer to these density profiles as the NFW, “steep,” and “shallow” profiles respectively. The motivation for using the shallow density profile is threefold. First, it is used to fit the inferred DM density distribution in some observed systems (e.g., de Blok et al. 2001). Second, it corresponds to a regime applicable for warm DM (WDM) and decaying DM (DDM) models, which would introduce such a core in the profile (e.g., Hogan & Dalcanton 2000; Avila-Reese et al. 2001). Third, it has been argued that the *extrapolated* density profiles of cosmological DM halos have cores and not cusps (Stoehr et al. 2002). It is worthwhile to stress again that in our modeling γ denotes the asymptotic slope of the density profile. Instead, the logarithmic slopes of the steep, NFW, and shallow profiles at 1% of r_{vir} are $d \ln \rho / d \ln r \simeq -1.72$, $\simeq -1.21$, and $\simeq -0.24$, respectively. Throughout the remainder of this paper we use the terms *inner* and *central* density slope to refer to the logarithmic slope of the spherically-averaged density profiles at the minimum resolved radii of the simulations.

Our choice of density slopes ensures that the employed density profiles have significantly different shapes, a fact which will be crucial for the interpretation of the results. Each of our initial DM halos had a virial mass of $M_{\text{vir}} = 10^{12} M_\odot$, implying a virial radius of $r_{\text{vir}} \simeq 256.7$ kpc, and a concentration of $c = 12$ (Bullock et al. 2001b), resulting in a scale radius of $r_s \simeq 21.4$ kpc. The adopted value of M_{vir} serves merely practical purposes and does not imply anything special about the particular choice of mass scale. Because we do not consider non-gravitational processes such as gaseous dissipation, the scale-free nature of gravity allows the rescaling of our models to any system of units and hence the extension of our conclusions to mergers between equal-mass systems of any mass scale.

The left panel of Figure 1 shows the density, $\rho(r)$, (*bottom panel*) and logarithmic slope profiles, $d \ln \rho(r) / d \ln r$, (*top panel*) for all initial halo models as a function of radius in units of the virial radius, r_{vir} . Density is given in units of the virial density, $\rho_{\text{vir}} \equiv \Delta_{\text{vir}} \rho_{\text{crit}}$. Thick lines correspond to the cumulative mass profiles for all initial halo models, $M(r)$, normalized to the virial mass, M_{vir} . We computed density profiles from the force resolution (2ϵ , where ϵ denotes the gravitational softening), outward defining the location of the most bound particle as the center of the system. To reduce noise, density profiles were averaged over 25 timesteps spanning a timescale equal to the crossing time at the virial radius of the system, $t_{\text{cross}}(r_{\text{vir}}) = \sqrt{r_{\text{vir}}^3/GM_{\text{vir}}}$. We derived logarithmic slope profiles by fitting the averaged density profile data

locally about each radius. The accuracy of the density slope calculation was tested by comparing the results of the local fits against the exact analytical expressions for the initial models. The adopted fitting procedure yielded maximum relative deviations of approximately 2%. This accuracy suffices for the purposes of our analysis.

2.2. Galaxy Models

Disk galaxy models are constructed according to the procedure described in Hernquist (1993) and their structural parameters are motivated by the currently favored galaxy formation paradigm in the standard Λ CDM model (Mo et al. 1998). Each disk galaxy model consists of a stellar disk embedded in a spherical and isotropic NFW DM halo. The stellar disks follow an exponential distribution in cylindrical radius R and their vertical structure is modeled by isothermal sheets

$$\rho_d(R, z) = \frac{M_d}{4\pi R_d^2 z_d} \exp\left(-\frac{R}{R_d}\right) \operatorname{sech}^2\left(\frac{z}{z_d}\right), \quad (7)$$

where M_d , R_d and z_d denote the mass, radial scale length, and vertical scale height of the disk, respectively. In our modeling, we parametrize the disk mass to be a fraction m_d of the halo virial mass, $M_d = m_d M_{\text{vir}}$, and we specify the disk vertical scale height in units of the radial disk scale length.

While most of the models used in this study do not contain a bulge, we also consider more general galaxy models that include a compact bulge component. For simplicity, we ignore any rotation in the bulges and model them as non-rotating spheroids that follow the Hernquist (1990) density profile

$$\rho_b(r) = \frac{M_b}{2\pi} \frac{a}{r(a+r)^3}, \quad (8)$$

where M_b is the bulge mass and a its scale length. In analogy to the treatment of the disk, we assume that the bulge mass is a fraction m_b of the halo virial mass, $M_b = m_b M_{\text{vir}}$, and parametrize the bulge scale length in units of the radial disk scale length, $a = f_b R_d$.

The DM halos are exponentially truncated beyond r_{vir} using equation (3) and have the same M_{vir} and c as the pure halo models. Once a set of cosmological parameters is adopted, the virial quantities M_{vir} and r_{vir} are uniquely determined by the halo circular velocity at the virial radius, V_{vir} (Mo et al. 1998). Furthermore, the DM halo carries some net angular momentum specified by the dimensionless spin parameter, $\lambda = J/G\sqrt{|E|/M_{\text{vir}}^5}$, where J and E are the total halo angular momentum and energy, respectively. We follow Springel & White (1999) and distribute the angular momentum of the DM halo by setting the halo streaming velocity to be a fixed fraction of the local total circular velocity. In our modeling, we assume that there is no exchange of angular momentum between the disk and the DM halo. We also assume no angular momentum exchange between the disk and the bulge during galaxy formation. Thus, the specific angular momentum content of the disk is conserved.

Finally, the DM halos are adiabatically contracted in response to the growth of the collisionless stellar components under the assumptions of spherical symmetry, homologous contraction, circular DM particle orbits, and angular momentum conservation (Blumenthal et al.

1986). The final DM distribution, $M_f(r)$, can then be derived from the initial mass profiles of DM, $M_{\text{DM}}(r)$, and baryons, $M_b(r)$, and the final baryon distribution, $M_b(r_f)$, according to

$$[M_{\text{DM}}(r) + M_b(r)] r = [M_f(r) + M_b(r_f)] r_f, \quad (9)$$

where r_f is the final radius of a DM particle. The right panel of Figure 1 displays the density and logarithmic slope profiles of DM after the growth of different stellar components. For comparison, we also show the DM distribution of the initial NFW profile before the baryonic infall. Adiabatic contraction modifies the DM density distribution significantly. The inner profile approaches a power law with $\rho(r) \propto r^{-2}$ after including both the disk and bulge components.

For all disk galaxy models considered here, we adopt a halo spin parameter equal to $\lambda = 0.031$, which is close to the mean value of spins measured in cosmological N -body simulations (e.g., Bullock et al. 2001a), a disk mass fraction of $m_d = 0.04$, and a constant vertical scale height across the disk equal to $z_d = 0.1 R_d$. When a bulge component is added, its mass and scale radius are specified by $m_b = 0.008$ and $f_b = 0.2$, respectively. The radial disk scale length R_d is uniquely determined for a given set of parameters M_{vir} , c , λ , m_d , m_b , and f_b . The resulting radial disk scale lengths are either $R_d = 3.8$ kpc or $R_d = 3.5$ kpc, depending on whether or not the galaxy models are bulgeless. All disk galaxy models are initially dynamically stable against bar formation (the mean Toomre Q -parameter of the disk was about 1.4) and their structural parameters are in accord with dynamical mass model A1 for the Milky Way presented in Klypin et al. (2002).

Particle positions for each component are initialized according to the analytic density profiles. For the particle velocities, we assume that the velocity distribution at any point in space is sufficiently well approximated by a multivariate Gaussian whose mean velocity and velocity dispersion tensor are given by the solution of the Jeans' equations at this point (see Hernquist (1993) for a detailed discussion of sampling velocities). A critical reader may note that disk galaxy models initialized under this scheme are not formally self-consistent. Most interesting galaxy and halo models have local self-consistent velocity profiles that become strongly non-Gaussian, especially near their centers. Indeed, Kazantzidis et al. (2004c) and Springel et al. (2005) performed numerical experiments of isolated, spherically-symmetric DM halos and established that the central density cusps relax rapidly to an inner slope significantly shallower than the slope that was initially intended (see Kazantzidis et al. (2004c) and Kazantzidis et al. (2004a) for a full discussion regarding the implications of such instabilities for the evolution of substructure in CDM halos and comparisons of the observed satellite dynamics with the predictions of CDM models).

While this is strictly correct, we argue that the galaxy models used in this study are not seriously affected by the approximate scheme that we employed. The reason is that the growth of different stellar components forces the inner DM density profile to approach a power law with slope $\gamma \sim -2$. As the central density cusp becomes closer to the $\rho(r) \propto r^{-2}$ profile of a singular isothermal sphere, the local velocity distribution approaches a Gaussian.

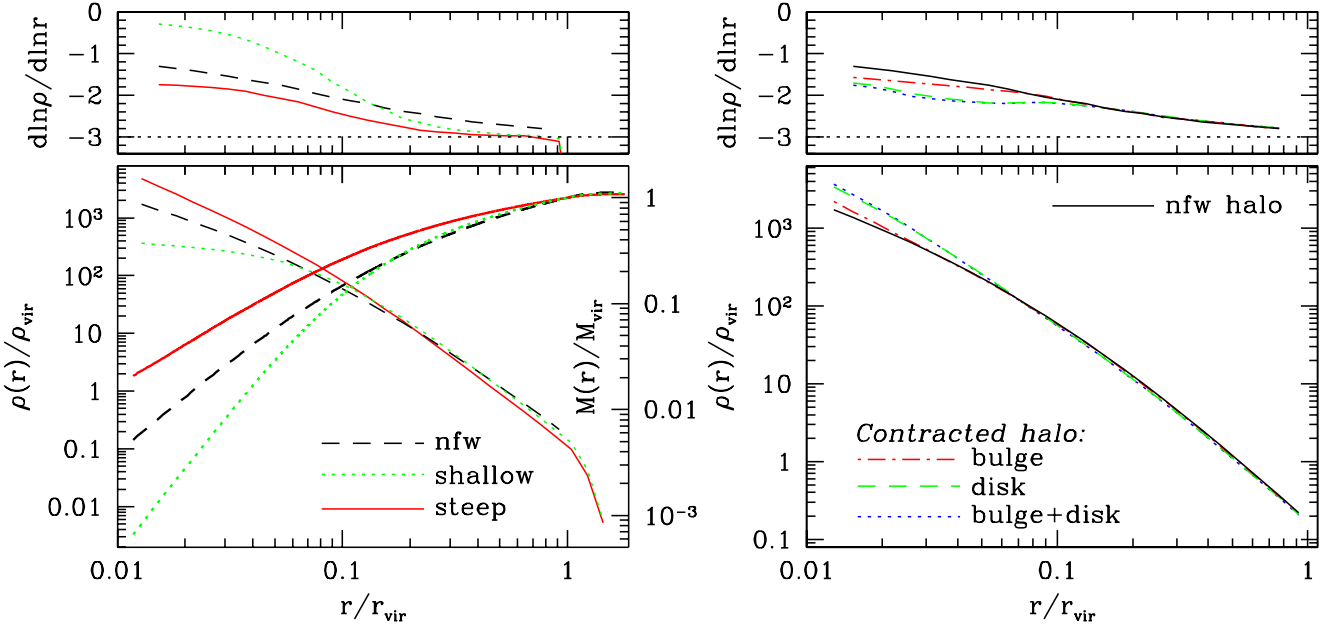


FIG. 1.— *Left:* Density, $\rho(r)$, (bottom panel) and logarithmic slope profiles, $d \ln \rho(r) / d \ln r$, (top panel) for initial halo models as a function of radius in units of the virial radius, r_{vir} . Density is normalized to the virial density, $\rho_{\text{vir}} \equiv \Delta_{\text{vir}} \rho_{\text{crit}}$. The solid, dashed, and dotted lines show results for the steep ($\gamma = 1.7$), NFW, and shallow ($\gamma = 0.2$) profiles, respectively. The initial density profiles are exponentially truncated beyond r_{vir} because they correspond to cumulative mass distributions that diverge at large radii. The density slope profiles are computed by fitting averaged density profiles locally at each radius. Thick lines correspond to cumulative mass profiles for initial halo models normalized to the virial mass, M_{vir} (right axis). *Right:* Density and logarithmic slope profiles of DM after adiabatic contraction of an NFW density profile in response to the growth of different stellar components. The profile before the baryonic infall corresponds to the solid curve. The dot-dashed, dashed, and dotted lines are the DM profile after the growth of a bulge, disk, and a bulge+disk with parameters equal to those of our fiducial disk galaxy model. The DM distribution responds in degrees to the size of the total stellar component included in the model and its central density profile approaches a power law with slope -2 after the inclusion of both disk and bulge.

In this case, the accuracy with which we compute the velocity distribution function is significantly improved. In fact, here we exploit the adiabatic contraction of the DM to construct *nearly* self-consistent disk galaxy models that do not show any discernible density evolution when evolved in isolation. We note that the numerical experiments of Kazantzidis et al. (2004c) adopted pure halo models with an inner cusp of $\rho(r) \propto r^{-1}$, whereas the simulations of Springel et al. (2005) considered compound galaxy models with a Hernquist DM halo and no adiabatic contraction.

For completeness, we also considered two-component elliptical galaxies comprised of a spherical non-rotating stellar distribution embedded in a spherical and isotropic NFW DM halo. The initial stellar distributions followed the Hernquist density profile. We constructed N -body models of elliptical galaxies adopting a procedure similar to the one described in Section 2.1 for the realization of self-consistent one-component halo models. Briefly, in order to embed spherical stellar distributions that are in equilibrium inside spherical DM halos, we simply need to calculate the DF of component i , $f_i(\mathcal{E})$. This is done by adding the appropriate potential term to equation (5)

$$f_i(\mathcal{E}) = \frac{1}{\sqrt{8\pi^2}} \int_0^{\mathcal{E}} \frac{d^2 \rho_i}{d\Psi^2} \frac{d\Psi}{\sqrt{\mathcal{E} - \Psi}}, \quad (10)$$

where ρ_i is the density profile of component i and $\Psi(r) = \psi_{\text{DM}}(r) + \psi_{\text{stars}}(r)$ is the total gravitational potential.

Finally, the elliptical galaxy models are constructed as before with the particle positions and velocities initial-

ized from the corresponding DF. Note that the density profile of the DM halo will be modified when the stellar distribution forms in its center and will no longer be described by equation (1). We explicitly take this into account when calculating the halo DF. Similar to the disk galaxy models, we computed the change in the halo density structure by assuming that it responds adiabatically to the growth of the stellar component and using the standard form of the adiabatic contraction model of Blumenthal et al. (1986).

Before adiabatic contraction, the DM halos of the elliptical galaxies had the same virial mass and concentration as the pure halo models, $M_{\text{vir}} = 10^{12} M_{\odot}$ and $c = 12$. The mass of the stellar distribution is chosen to be $M_{\text{stars}} = 0.1 M_{\text{vir}}$. In order to assign the remaining free parameter of the Hernquist profile, namely the scale length a , we followed Boylan-Kolchin et al. (2005) and used the observed relation between stellar mass and effective radius R_e for early-type galaxies in the Sloan Digital Sky Survey data (Shen et al. 2003),

$$R_e = 4.16 \left(\frac{M_{\text{stars}}}{10^{11} M_{\odot}} \right)^{0.56} \text{kpc}. \quad (11)$$

For the Hernquist profile, the effective radius R_e is related to the scale length a by $R_e \approx 1.82a$, giving $a \approx 2.3$ kpc for our main elliptical galaxy model. In the following section, we present a detailed description of all of the merger simulations that we undertake in this study.

TABLE 1
SUMMARY OF MERGER SIMULATIONS

| Model | Initial Models | | | | Remnants | | |
|------------------|----------------|------------|-----------|--|---|-----------------------------|--|
| | γ_1 | γ_2 | Orbit | $ \mathrm{d} \ln \rho / \mathrm{d} \ln r $ | M_{vir} ($10^{12} M_{\odot}$) | r_{vir} (kpc) | $ \mathrm{d} \ln \rho / \mathrm{d} \ln r $ |
| (1) | (2) | (3) | (4) | (5) | (6) | (7) | (8) |
| HRBp | 1 | 1 | Parabolic | 1.16 | 1.42 | 288.7 | 1.13 |
| Bp1 | 1 | 1 | Parabolic | 1.31 | 1.42 | 288.7 | 1.30 |
| Bp2 | 0.2 | 0.2 | Parabolic | 0.29 | 1.42 | 288.7 | 0.28 |
| Bp3 | 1.7 | 1.7 | Parabolic | 1.74 | 1.56 | 297.7 | 1.73 |
| hBp1 | 0.2 | 1 | Parabolic | 0.29, 1.31 | 1.42 | 288.8 | 1.23 |
| hBp2 | 0.2 | 1.7 | Parabolic | 0.29, 1.74 | 1.48 | 292.5 | 1.70 |
| Br1 | 1 | 1 | Radial | 1.31 | 1.62 | 301.5 | 1.28 |
| Br2 | 0.2 | 0.2 | Radial | 0.29 | 1.61 | 301.1 | 0.28 |
| Br3 | 1.7 | 1.7 | Radial | 1.74 | 1.68 | 305.1 | 1.73 |
| hBr1 | 0.2 | 1 | Radial | 0.29, 1.31 | 1.62 | 301.4 | 1.21 |
| hBr2 | 0.2 | 1.7 | Radial | 0.29, 1.74 | 1.62 | 301.6 | 1.70 |
| Bc1 | 1 | 1 | Circular | 1.31 | 1.54 | 296.5 | 1.28 |
| Bc2 | 0.2 | 0.2 | Circular | 0.29 | 1.57 | 298.4 | 0.28 |
| Bc3 | 1.7 | 1.7 | Circular | 1.74 | 1.55 | 297.2 | 1.73 |
| hBc1 | 0.2 | 1 | Circular | 0.29, 1.31 | 1.53 | 296.0 | 1.22 |
| hBc2 | 0.2 | 1.7 | Circular | 0.29, 1.74 | 1.52 | 295.2 | 1.70 |
| Qp1 | 0.2 | 0.2 | Parabolic | 0.29 | 3.24 | 380.0 | 0.27 |
| Qp2 | 1.7 | 1.7 | Parabolic | 1.74 | 3.31 | 382.8 | 1.72 |
| Qr1 | 0.2 | 0.2 | Radial | 0.29 | 3.15 | 376.4 | 0.27 |
| Qr2 | 1.7 | 1.7 | Radial | 1.74 | 3.26 | 380.8 | 1.72 |
| Sp1 | 1 | 1 | Parabolic | 1.31 | 1.94 | 320.5 | 1.28 |
| Sp2 | 1 | 1 | Parabolic | 1.31 | 2.61 | 353.6 | 1.27 |
| Sp3 | 0.2 | 0.2 | Parabolic | 0.29 | 1.80 | 312.1 | 0.26 |
| Sp4 | 0.2 | 0.2 | Parabolic | 0.29 | 2.21 | 334.7 | 0.25 |
| Sp5 | 1.7 | 1.7 | Parabolic | 1.74 | 2.35 | 341.5 | 1.72 |
| Sp6 | 1.7 | 1.7 | Parabolic | 1.74 | 3.09 | 373.9 | 1.71 |
| egBp | 1 | 1 | Parabolic | 2.03 | 1.30 | 280.5 | 2.01 |
| hbBp | 1 | 1 | Parabolic | 1.57 | 1.40 | 287.5 | 1.55 |
| dgBp1 (coplanar) | 1 | 1 | Parabolic | 1.70 | 1.38 | 286.1 | 1.69 |
| dgBp2 (inclined) | 1 | 1 | Parabolic | 1.70 | 1.39 | 286.6 | 1.69 |
| dgBr (inclined) | 1 | 1 | Radial | 1.70 | 1.54 | 296.7 | 1.69 |
| hbdBp (inclined) | 1 | 1 | Parabolic | 1.76 | 1.38 | 286.1 | 1.74 |

NOTE. — Columns (1)-(5) refer to the properties of the initial models. Columns (6)-(8) refer to the properties of the merger remnants. The quantities in each column are as follows. Col. (1): Abbreviations for the merger simulations, B = binary, Q = quadruple, S = sequential, p = parabolic, r = radial, c = circular, h = hybrid, eg = elliptical galaxy, dg = disk galaxy consisting of a halo and a disk, hb = galaxy consisting of a halo and a bulge, hbd = galaxy consisting of a halo, a disk, and a bulge. For mergers between galaxies containing disks the orientation of the merging disks is included in parentheses. All initial halo models have $N = 2 \times 10^5$ particles except for run HRBp which refers to the high-resolution binary, parabolic merger between NFW halos with $N = 2 \times 10^6$ particles per progenitor. Col. (2), (3): Asymptotic inner density slopes. Note that for galaxy models the asymptotic inner density slope of the initial *uncontracted* NFW halo model is given. Col. (4): Initial orbital configuration. Col. (5): Logarithmic density slope at the *minimum* resolved radii. For mergers of identical progenitors only one number is shown while for the hybrid mergers of two different initial models, two slopes are given. For the galaxy models we only give the density slope of the DM component. We estimate that our determination of slopes is accurate to within $\sim 2\%$ at radii that are well resolved. Col. (6): Virial mass in units of $10^{12} M_{\odot}$. Col. (7): Virial radius in kpc. Col. (8): Logarithmic slope at the innermost resolved radius.

2.3. Description of Merger Simulations

All numerical calculations discussed in this paper were carried out using PKDGRAV, a multi-stepping, parallel, tree N -body code (Stadel 2001). PKDGRAV uses a spline softening length, such that the force is completely Keplerian at twice the quoted softening length, and multi-stepping based on the local acceleration of particles. We used an adaptive, kick-drift-kick leapfrog in-

tegrator with individual particle time steps Δt_i chosen according to $\Delta t_i \leq \eta(\epsilon_i/\alpha_i)^{1/2}$, where ϵ_i is the gravitational softening length of the particle, α_i is the value of the local acceleration, and η is a parameter that specifies the size of the individual timesteps and consequently the time accuracy of the integration.

2.3.1. Numerical Parameters

For all merger simulations between pure DM halos, we used $N = 2 \times 10^5$ particles and employed a gravitational softening length of $\epsilon = 1.5$ kpc. This choice enables us to resolve density profiles to $\sim 1\%$ of the virial radii of the simulated systems. The adopted force resolution is comparable to the mean particle separation within the region we want to resolve and is in accord with recent studies suggesting optimal scalings between the number of particles, N , and the minimum resolved radii (e.g., Power et al. 2003; Reed et al. 2005). In § 2.4, we quantify the numerical effects of two-body relaxation on the central regions of our models and conduct convergence tests to ensure that the adopted mass and force resolution is adequate for the purposes of this study. The results of these tests confirm that our N -body simulations are robust to artificial numerical effects.

For binary mergers between multicomponent systems, we used $N = 2 \times 10^5$ particles to represent the DM halo and $N = 2 \times 10^4$ collisionless stellar particles for each stellar component. Gravitational forces for the stellar components were computed using a softening length of $\epsilon = 0.25$ kpc and the force resolution of the DM component was the same as in the halo-only mergers. To quantify the extent of artificial numerical effects on our findings, we compared the results of these merger simulations against the higher resolution calculations presented in the study of Kazantzidis et al. (2005). These authors employed galaxy models consisting of 10^6 DM particles and 10^5 particles in each stellar component and correspondingly smaller softening lengths. The comparison showed excellent agreement and in the remainder of the paper we will always present results for merger simulations with the standard mass and force resolution.

For all simulations, we set the base-timestep to be equal to 1% of the dynamical time at the half-mass radius of the model and allowed the individual particle timesteps to be at most a factor of 2^{30} smaller. The time integration was performed with high enough accuracy such that the total energy was conserved to better than 0.1% in all cases, which is adequate for the type of study that we undertake in this paper. As we have already stated, one of our main goals is to investigate the evolution of the central density slopes on small scales. The total energy contained in the inner regions of our models is a few tens of a percent of that of the entire system, so the energy conservation accuracy must be at least comparable to that in order to resolve meaningfully the dynamics of the region of interest.

2.3.2. Orbital Parameters

Initial conditions for binary mergers were generated by building pairs of halo or galaxy models and placing them at a distance equal to twice their virial radii. In the coordinate system chosen to describe the merger simulations, the orbital plane coincides with the $x - y$ plane, and the center of mass of the system coincides with the coordinate origin. We simulated binary mergers of systems on parabolic orbits in agreement with cosmological expectations (e.g., Khochfar & Burkert 2005). In order to examine the effect of encounter geometry and initial orbital energy on the density structure of the merger remnants we also considered circular orbits and radial orbits with zero orbital angular momenta (Moore et al. 2004).

For the parabolic mergers, we set the initial models on

orbits with pericentric distances of 20% of the halo virial radii, a value that is typical of merging halos in cosmological simulations (e.g., Ghigna et al. 1998; Zentner et al. 2005; Benson 2005). The initial center of mass velocity of each pair was determined from the corresponding Keplerian orbit of two point masses. The trajectories of the merging systems deviate shortly after they begin to overlap as orbital energy is dissipated and eventually follow closer orbits. In the case of the radial mergers, we set the initial relative velocities to be equal in magnitude to the velocities of point particles in a circular orbit about the common center of mass. In this way, both the radial and circular mergers have precisely the same total orbital energy.

For binary mergers between disk galaxy models it is also necessary to choose a relative orientation for the disk components. We simulated parabolic and radial mergers using both randomly-inclined and coplanar prograde (disk spin vectors parallel to the orbital angular momentum vector) disk orientations. A subset of these binary merger simulations were discussed in Kazantzidis et al. (2004a) where additional details can be found. Finally, we performed a single parabolic binary merger between elliptical galaxies aimed at establishing the generality of our basic conclusions.

Besides conducting binary mergers, one of our additional goals was to assess the net effect of a *hierarchy* of mergers, which is a more appropriate characterization of the early evolution of halos in the standard paradigm of cosmological structure formation. Along these lines, we have simulated a sequence of binary, equal-mass mergers between identical halos for each of the shallow, NFW, and steep initial density profiles. For this ensemble of simulations we only utilized parabolic orbits. Each sequence of mergers consisted of three simulations. The first stage was simply the binary merger between the initial halo models described above. In the second stage, we merged identical copies of the merger remnants from the first stage. We identified a time after which the central density profile of the remnant did not evolve significantly (changes of the order of 1 – 2% were considered acceptable) and removed all unbound particles. We underscore that the outer regions of remnants may evolve for much longer (e.g., Kazantzidis et al. 2004a) as density waves associated with the merger process may persist for an extended period of time after the cores of the halos coalesce and the merger would conventionally be deemed complete. Finally, we chose the initial relative orientation of the principal axes of the remnants randomly, placed the remnants at a relative distance equal to twice their virial radii, and set them on parabolic orbits. For the third stage, we repeated the previous process using as progenitor systems the remnants of the previous stage.

We determined the bound mass in each of the remnants using the iterative scheme described in Kazantzidis et al. (2004c). In the rest frame of the most bound particle, we calculated the binding energies of all other particles using the tree-based gravity calculation performed by PKDGRAV and we removed all particles with positive binding energy. We repeated this calculation of binding energies and subsequent removal of unbound particles until no more unbound particles were found. In practice this iterative procedure converges rapidly and ensures that the true, bound entity will be identified. This tech-

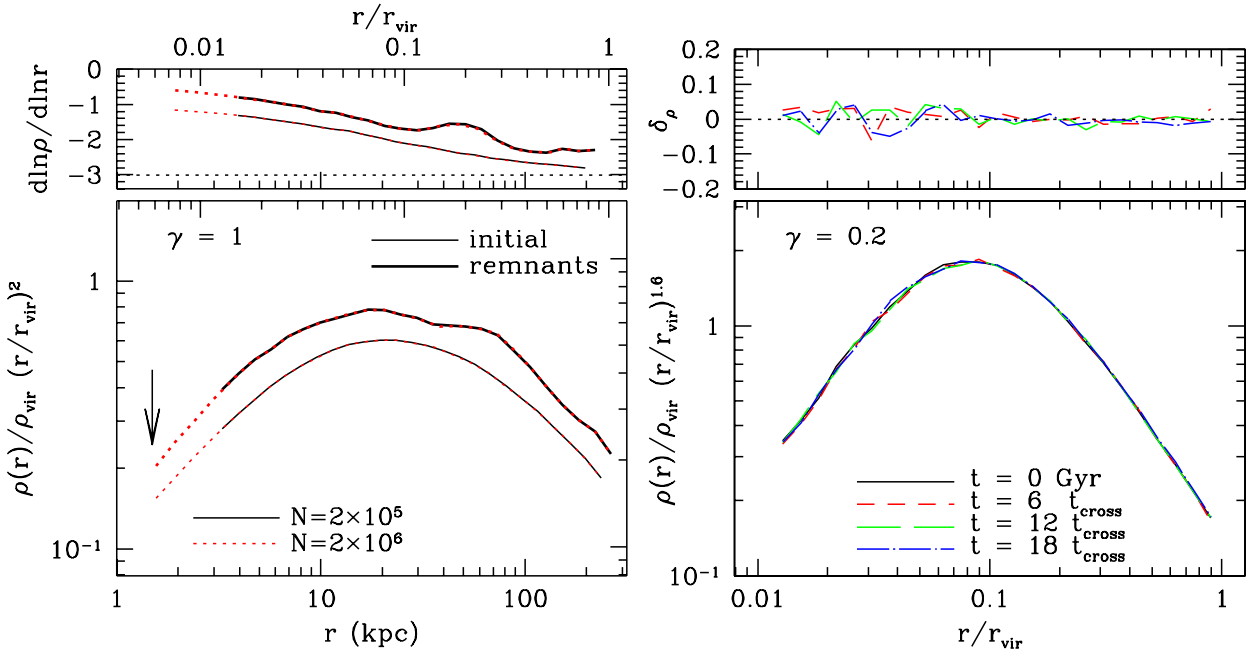


FIG. 2.— *Left:* Spherically-averaged density, $\rho(r)$, (*bottom panel*) and logarithmic slope profiles, $d \ln \rho(r) / d \ln r$, (*top panel*) for two binary, parabolic merger simulations between NFW halos. Each simulation has a different force and mass resolution. In order to highlight any differences at small radii, we plot the product $\rho(r)r^2$, which is constant for isothermal distributions. The density profiles are plotted from the force resolution (2ϵ) outward and the number of particles, N , is indicated in the *lower left-hand corner*. Radius is shown in both physical units (*bottom axis*) and as a fraction of the virial radius of the *initial* models, r_{vir} (*top axis*). For clarity, the density slopes corresponding to the remnants (*thick lines*) have been shifted up by 0.5 dex. The downward arrow indicates the gravitational softening used in the low-resolution simulation. The profiles are indistinguishable from the radius corresponding to the force resolution of the lower resolution simulation indicating that numerical convergence has been achieved. *Right:* Density profile as a function of time spanning $18 t_{\text{cross}}(r_{\text{vir}})$ for an isolated halo following the shallow density profile. In order to emphasize any differences at small radii, we plot the product $\rho(r)r^{(\beta+\gamma)/2}$. The maximum of this quantity indicates the scale radius of the system. *Top panel:* Relative density differences, δ_ρ , between the initial, ρ_{in} , and final, ρ_{fi} , profiles for the same timescales. Virtually no evolution in the density profile can be discerned over the timescales of the simulation, indicating that our numerical results are robust against two-body relaxation for evolution on timescales smaller than $18 t_{\text{cross}}(r_{\text{vir}})$.

nique is essentially the same used in most group-finding routines, like the publicly-available SKID (Stadel 2001), but has the advantages of using a tree structure for the potential computation, which requires $\mathcal{O}(N \log N)$ operations instead of $\mathcal{O}(N^2)$ for N particles, and a parallel implementation for very large N . In this way, a much larger number of particles can be used in the calculation than would be possible with SKID at a fraction of the computational burden.

In addition, we considered the simultaneous merging of four systems. Initial conditions for these quadruple mergers were generated by building halo pairs identical to the ones used in the binary merger experiments. We considered only shallow and steep initial density profiles, as these are the extremes of the range of profiles that we studied with the binary merger experiments, and set the center of mass position and velocity of the first pair to be the same as in the binary merger experiments. For the second pair, we changed the signs of the center of mass coordinates of each halo in such a way that its orientation was rotated 90° with respect to the first pair. We simulated quadruple mergers in which each pair was initially set on either a parabolic or a radial orbit. The trajectories of the merging systems will strongly deviate from a parabolic and radial orbit shortly after the beginning of the simulation, but here we are not interested in reproducing a particular orbital configuration. The setup

of these experiments simply ensures that four halos that correspond to the steep and shallow density profiles will merge following orbits with very different orbital configurations and orbital energies. However, for convenience, we shall refer to these quadruple mergers as “parabolic” and “radial”.

In addition to the DM-only halo mergers, we studied the merging of the multicomponent galaxy models described in § 2.2. We studied mergers of identical galaxies with stellar disks and bulges embedded in adiabatically contracted DM halos as well as mergers of galaxies with only stellar disks or bulges. For the halo+disk mergers, we studied variations in both the initial orbital configuration and the initial relative orientation of the stellar disks. We considered mergers of disks randomly inclined with respect to the orbital plane on both parabolic and radial initial orbits and mergers of coplanar prograde disks on parabolic initial orbits. For the mergers of halo+disk+bulge compound galaxy models the stellar disks were randomly inclined and the initial orbit was parabolic. Finally, for the halo+bulge and elliptical galaxy mergers, parabolic was again the initial orbit of choice. Table 1 contains a summary of all merger simulations performed in this study and a list of parameters and variables for all initial models and remnants.

2.4. Numerical Tests

In order to minimize any concern that our results might be compromised by artificial numerical effects, we performed experiments varying the mass resolution by a factor of 10 and scaling down the softening lengths according to $\epsilon \propto N^{-1/3}$. Results from one of these tests are displayed in the left panels of Figure 2. Although the merger remnants exhibit significant departures from spherical symmetry, it is instructive to calculate spherically-averaged remnant density profiles. Fig. 2 shows *average* density $\rho(r)$, and logarithmic slope profiles $d \ln \rho(r) / d \ln r$, for two parabolic, binary mergers between NFW halos at two different numerical resolutions. The agreement in the density and logarithmic slope profiles of the remnants simulated at different resolutions indicates that numerical convergence has been achieved.

Two-body relaxation is a numerical artifact associated with the use of particles to sample phase-space in the collisionless limit. The coarse-grained sampling of phase-space originating from the enormous difference between the mass of a particle in N -body simulations and that of DM particle candidates results in a mean potential that can be dominated by two-body interactions. As a result, two-body relaxation sets a limit on the region of an N -body system within which the numerical results can be trusted. All of our initial models have a central density slope shallower than that of an isothermal ($\rho \propto r^{-2}$) model, therefore energy transfer due to two-body relaxation would cause an expansion of the central region and a subsequent flattening of the inner density slope, potentially interfering with the interpretation of our results.

To thoroughly investigate the effects of two-body relaxation on our results, we performed a test simulation. We evolved a halo in isolation following the shallow density profile for a total elapsed time of $t_{\text{relax}} = 18 t_{\text{cross}}(r_{\text{vir}})$. For the particular model we studied this corresponds to $t_{\text{relax}} \simeq 34$ Gyr. The results of this experiment are shown in the right panels of Figure 2. These panels present the density profiles, $\rho(r)$, (*bottom panel*) and the relative density differences, $\delta_\rho = (\rho_{\text{in}} - \rho_{\text{fi}}) / \rho_{\text{in}}$, (*top panel*) between the initial ρ_{in} , and final ρ_{fi} , profiles as a function of time. The density differences are small (of the order of a few percent), indicating that discreteness effects associated with the finite number of particles do not cause this particular halo model to evolve away from its equilibrium configuration over these timescales. We stress that this shallow halo model will be the *most* susceptible to two-body relaxation owing to the relatively small number of particles in its central region. Therefore, we anticipate that all of our simulations should be unaffected by numerical relaxation for evolution on timescales that are smaller than t_{relax} above.

3. RESULTS

3.1. Binary Halo Mergers

We begin with the binary merger simulations between pure DM halos. In all parabolic and radial mergers, the systems merge in three to five orbits (between ~ 5 to ~ 7 Gyr), with the specific value depending on the inner power-law indices of the systems and the initial orbital configurations of the mergers. These timescales are larger than those reported in earlier studies of binary equal-mass mergers (e.g., Barnes & Hernquist 1996) due to the larger and more realistic pericentric distances

adopted here. The merger timescale is set by the combination of dynamical friction, which dissipates the orbital energy of the dense halo cores, and mass loss processes (e.g., Taffoni et al. 2003). Models with steeper inner density distributions merge faster due to the stronger gravitational drag exerted by the galaxy cores. The differences in merging times can be of the order of ~ 1 Gyr or even larger between shallow and steep density profiles. Finally, for circular orbits the merger process takes substantially longer time to complete owing to the much slower rate at which orbital energy is dissipated.

The first results that we present are those of the binary mergers involving identical halo models. In Figure 3, we show the spherically-averaged density, $\rho(r)$, (*bottom panels*) and logarithmic slope profiles, $d \ln \rho(r) / d \ln r$, (*top panels*) of the remnants for all nine identical-halo mergers along with the initial density profiles of each model. Note that each of the remnant profiles is normalized to its own virial radius, r_{vir} , as defined in § 2.1. Figure 3 demonstrates that the remnant density distributions, and particularly their inner power-law indices, are strikingly similar to those of the progenitor halos. This basic result holds for all initial density profiles and orbital energies that we considered.

Figure 4 presents cumulative mass profiles, $M(r)$, for the same set of binary merger simulations. The left and middle panels show mass profiles for mergers of identical initial halo models, while the right panel corresponds to the “hybrid” halo mergers which we will discuss in more detail below. Clearly, the cumulative measure reveals comparably less about the details of the inner density profiles, but this plot does display an interesting fact. The merger remnants contain significant fractions of their bound mass, ~ 25 – 35% as opposed to $\sim 10\%$ for the initial models, outside of what we formally identify as their virial radii. Parabolic orbits result in a larger fraction of particles outside r_{vir} compared to bound orbits owing to the fact that there is a larger amount of energy available to distribute in the former (see also Table 1). These particle fractions are consistent with studies of halos in cosmological simulations that find that equilibrium density profiles extend well beyond halo virial radii (Prada et al. 2005).

One of the practical consequences of this result concerns the ambiguous definition of the virial mass and the evolution of the virial mass in analytic models for galaxy and halo formation (e.g., Somerville & Primack 1999; Zentner & Bullock 2003; Benson et al. 2003; Taylor & Babul 2004; Zentner et al. 2005). The results reported in Figure 4 illustrate that a non-negligible amount of DM in the initial halo models is heated outside of the virial radius of the remnant. In fact, a few percent of the initial mass of the halos (between ~ 1 – 3%) becomes unbound in typical halo mergers.

Analytic models typically adopt a particular definition of halo virial mass and then assume that the virial mass is strictly additive during mergers. In contrast, the mass profiles in Figure 4 show that, for a common definition of the virial radius, the virial mass of the remnant is not simply the sum of the virial masses of the progenitors. This suggests that a more sophisticated approach is warranted in semi-analytic calculations that use extended Press-Schechter merger trees to follow the mass assembly histories of halos.

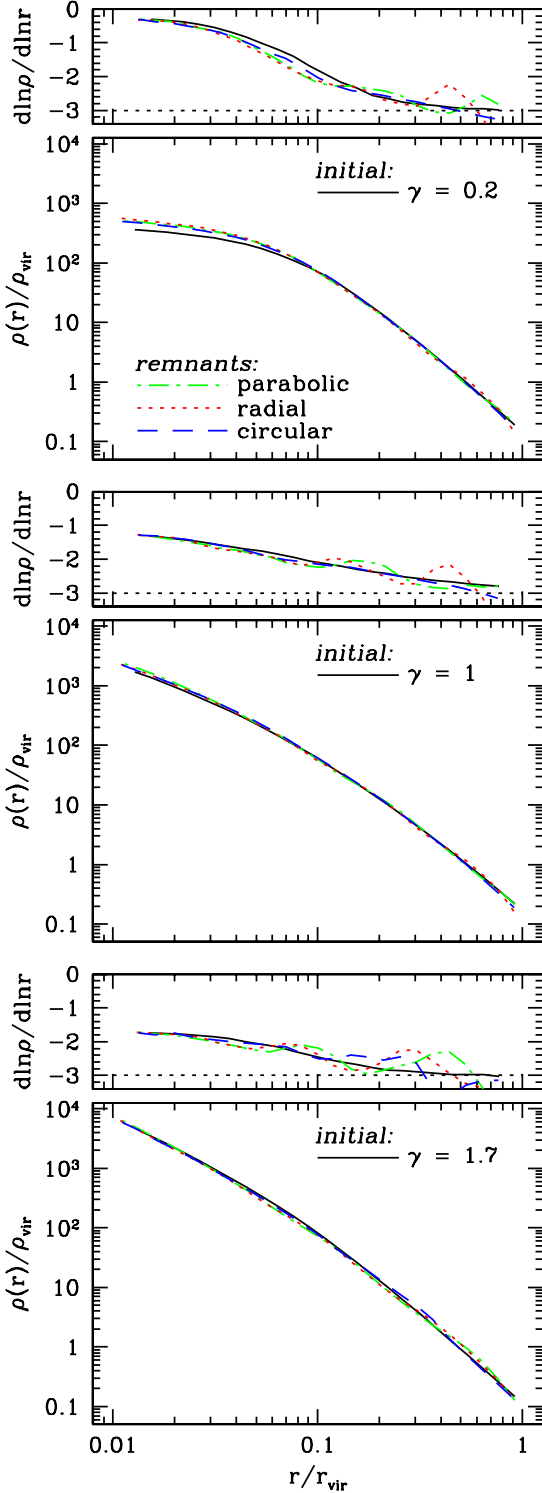


FIG. 3.— Spherically-averaged density and logarithmic slope profiles for initial systems (solid lines) and remnants in binary merger simulations between identical DM halo models. The profiles are plotted as a function of radius in units of the virial radius and each of the remnant profiles is normalized to its own r_{vir} . The asymptotic density power-law index, γ , of the initial profiles is indicated in the upper right-hand corner of each bottom panel. The dot-dashed, dotted, and dashed lines correspond to remnants in the parabolic, radial, and circular initial orbital configurations, respectively.

Following up on the findings reported in Figs. 3 and 4, are the results of the hybrid binary merger simulations in which we merged DM halo-only models with substantially different values of the asymptotic density power-law index, γ . The density profiles that result from the hybrid merger simulations are shown in Figure 5. This Figure reveals that, in equal-mass mergers between halos with different power-law central density indices, the remnant has a profile with an inner slope close to that of the steepest of the progenitors (see also Fulton & Barnes 2001; Boylan-Kolchin & Ma 2004). Similar to the DM halo-only mergers of identical initial models, this result is independent of the precise value of the initial inner power-law slopes and the initial orbital energy of the progenitor halos. In the hybrid mergers, the net result appears to be that the inner core of the steepest of the two initial systems survives essentially intact in the remnant, an effect noted previously by Boylan-Kolchin & Ma (2004) for mergers between NFW halos and halos with an inner core of constant density.

It is interesting to stress that the isodensity contours in the inner region $r \lesssim 0.1r_{\text{vir}}$ of a hybrid merger remnant are nearly spherical (both b/a and c/a , where $a \geq b \geq c$ are the principle axis ratios, are larger than 0.8). Strongly prolate remnants are emblematic of parabolic and radial mergers similar to the ones simulated here (e.g., Moore et al. 2004; Kazantzidis et al. 2004a). The almost spherical inner regions of the hybrid merger remnants lends support to the idea that the steepest inner spherical core survives, almost unaltered, in the center of the final system.

In Figure 6, we address the relative contribution of the progenitor halos to the remnant density profiles in *parabolic* mergers. In the left panel we show the quantity $\Delta\rho \equiv \rho_{\text{rem}}(r)/2\rho_{\text{in}}(r)$, where $\rho_{\text{rem}}(r)$ and $\rho_{\text{in}}(r)$ denote the densities of remnants and initial models, respectively. In the hybrid mergers, we have defined the fiducial quantity $2\rho_{\text{in}}(r) \equiv \rho_{\text{in}}^{\gamma_1}(r) + \rho_{\text{in}}^{\gamma_2}(r)$, where $\rho_{\text{in}}^{\gamma_1}(r)$ and $\rho_{\text{in}}^{\gamma_2}(r)$ correspond to the initial density profiles of the two systems and $\gamma_1 < \gamma_2$. In the right panel, we show the relative contribution of the progenitor halos to the cumulative mass profiles of the remnants, $\Delta M \equiv M_{\gamma_1}(r)/M_{\text{rem}}(r)$. Here $M_{\text{rem}}(r)$ is the total mass of the remnant and $M_{\gamma_1}(r)$ denotes the mass in the remnant that belongs to the progenitor halo with inner power-law index γ_1 .

As anticipated, in mergers of identical progenitor halos, the contribution to the remnant from each halo is equal by symmetry, but the variations in these quantities indicate the size of variations that are to be expected from numerical noise. For the hybrid encounters, the mass from the steeper progenitor dominates the inner regions ($r \lesssim 20$ kpc for the $[\gamma_1, \gamma_2] = [0.2, 1.0]$ merger and $r \lesssim 60$ kpc for the $[\gamma_1, \gamma_2] = [0.2, 1.7]$ merger) of the final density profiles. For example, in the $[\gamma_1, \gamma_2] = [0.2, 1.0]$ merger, 80% of the mass within the inner 10 kpc of the remnant originated from the NFW halo, while in the $[\gamma_1, \gamma_2] = [0.2, 1.7]$ merger, the steep halo contributes fully 90% of the remnant mass out to a distance of more than 20 kpc from the center of the remnant halo. Figure 6 also illustrates the fact that the resulting remnant profile is not simply a sum of the two profiles of the progenitors. The density of the remnant everywhere within the virial radius is smaller than twice the density of the

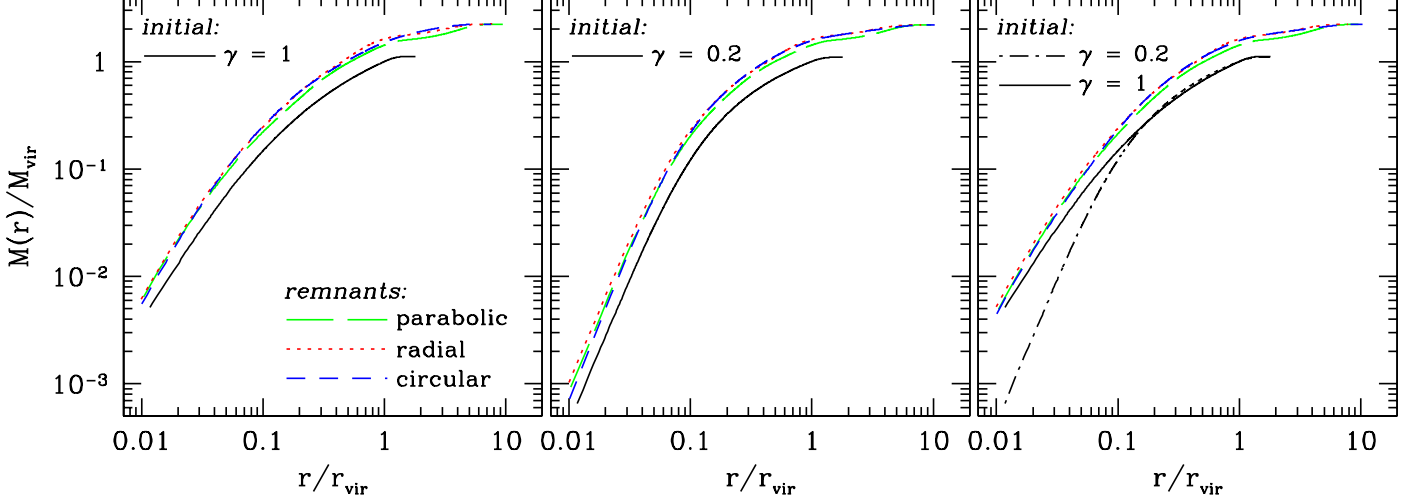


FIG. 4.— Cumulative mass profiles for remnants in binary merger simulations between halos as a function of radius in units of r_{vir} . All profiles are normalized to the virial mass of the *initial* halo models, M_{vir} . The two leftmost panels correspond to mergers between identical halo models with the initial value of γ indicated in the *upper left corners*. The cumulative mass profiles of the initial halos are shown by the *solid* lines. The right panel corresponds to a hybrid merger between an NFW halo (*solid* line) and a halo following the shallow density profile (*dashed* line). The different remnants correspond to different initial orbital configurations. The mass distribution of merger remnants extends well beyond the virial radius (note that $\gtrsim 90\%$ of mass in the initial models is contained within r_{vir}).

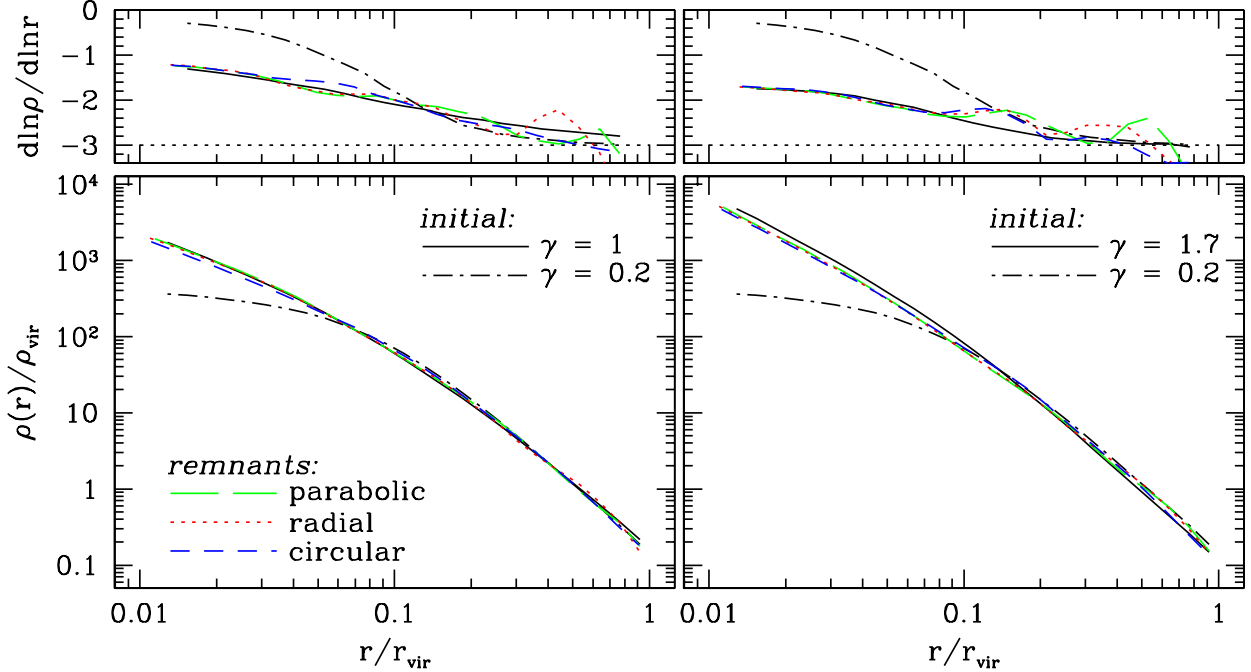


FIG. 5.— Density and logarithmic slope profiles as in Figure 3, but for binary mergers between halos with *different* initial central density power-law indices γ . The initial asymptotic density slopes are indicated in the *upper right corners* of the bottom panels. The steeper of the two initial profiles in each case is shown by the *solid* lines while the shallower of the two initial profiles is depicted by the *dot-dashed* lines.

initial models. This is because, as we noted above, mass is dynamically heated during the relaxation accompanying the merger and subsequently moves to larger radii.

3.2. Sequential and Multiple Halo Mergers

Next, we consider the merger sequences. In the sequential merger simulations, identical copies of the remnants from the identical halo mergers discussed in § 3.1 were collided with each other after removing the small number ($\sim 1 - 3\%$ in all cases) of unbound particles. We initial-

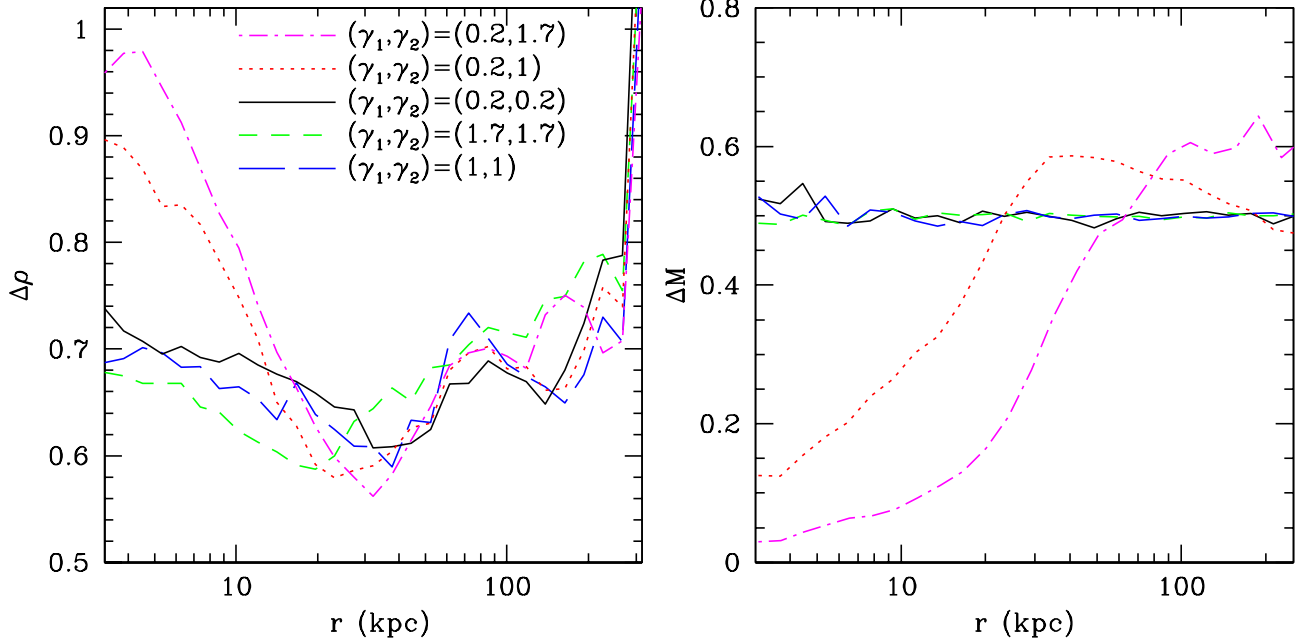


FIG. 6.— *Left:* Density fraction, $\Delta\rho \equiv \rho_{\text{rem}}/2\rho_{\text{in}}$, in binary, parabolic mergers between halos as a function of radius in absolute units. Here ρ_{rem} and ρ_{in} denote the densities of remnants and initial models, respectively. In mergers between systems with different asymptotic central density power-law indices, γ_1 and γ_2 , we define the fiducial quantity $2\rho_{\text{in}} \equiv \rho_{\text{in}}^{\gamma_1} + \rho_{\text{in}}^{\gamma_2}$, where $\rho_{\text{in}}^{\gamma_1}$ and $\rho_{\text{in}}^{\gamma_2}$ denote the initial density profiles of the two systems and γ_1 corresponds to the smaller asymptotic power-law slope. *Right:* Relative contribution of mass in the remnants of binary, parabolic mergers as a function of radius in physical units. ΔM is defined as $\Delta M \equiv M_{\gamma_1}(r)/M_{\text{rem}}(r)$, where $M_{\text{rem}}(r)$ is the total mass of the remnant and $M_{\gamma_1}(r)$ denotes the mass of the progenitor halo with an asymptotic power-law index γ_1 in the remnant. Line types are as in the left panel.

ized the mergers on parabolic orbits, placed the systems at relative distances equal to twice their virial radii and oriented the principal axes of the merger remnants randomly with respect to each other. We repeated this process again to yield a sequence of three merger remnants. We shall refer to the three levels of mergers as “level one,” “level two,” and “level three,” respectively. The level one mergers refer simply to the parabolic mergers discussed in § 3.1. Note that the pericentric distances for all merger levels are kept equal to 20% of the halo virial radii. This choice is motivated by the results of the binary merger simulations which demonstrated that the density structure of the remnants is largely insensitive to the details of the encounter orbital energy.

In all sequences of mergers, we identified a time after which the central density profile of the remnant did not evolve significantly (as before changes of the order of few percent were considered acceptable). We further allowed the remnants to settle into equilibrium for a timescale equal to one crossing time at the virial radius of the system, $t_{\text{cross}}(r_{\text{vir}})$. Then their equilibrium state was analyzed. The density profiles and logarithmic slopes for two of the remnant hierarchies, starting from the shallow and steep initial profiles, are shown in Figure 7. In order to reduce the noise in the measurement, we superposed the outputs from 25 snapshots between the time at which the merger was completed t_{comp} , and $t_{\text{comp}} + t_{\text{cross}}(r_{\text{vir}})$. Not surprisingly, the remnants at all levels of the hierarchy exhibit faithful memories of the inner power-law indices of their progenitors. This indicates that, even in a complex hierarchy of halo mergers, the inner slopes of the density profiles are well preserved. Repeated dis-

sipationless equal-mass merging cannot modify the inner power-law index or even the general shape of the spherically-averaged density profiles. The evolution of the virial mass in these simulations of hierarchical merging is even stronger than the one portrayed in the binary encounters. Indeed, the fraction of particles found outside of what is formally identified as r_{vir} rises to $\sim 50\%$ in the third level of mergers, emphasizing the need for more reliable accounting in semi-analytic models.

Following up on the evolution of the profile shapes, an intriguing result of the sequential merger experiments is reported in Figure 8. Here, we plot the product $r^{(\beta+\gamma)/2}\rho(r)$, where radii and densities are normalized to the virial values, as a function of r/r_{vir} . The quantity $(\beta+\gamma)/2$ is equal to 1.6, 2.0, and 2.35 for the shallow, NFW, and steep profiles respectively. There are several reasons to plot this quantity. First, it scales out the gross dependence of the halo profile on radius so that small changes become more apparent. Second, the radius at which this quantity is maximized corresponds to the scale radius, r_s , of the density distribution. The three panels of Figure 8 show that the general shape of the remnant density profiles changes minimally throughout the merging sequence. In particular, the scale radius appears to remain fixed at a nearly *constant fraction* of the virial radius of the halo at all stages. In other words, the concentration parameter remains approximately constant during periods of equal-mass merging.

The strongest evolution appears to be between the initial and the level one merger remnant profiles. However, this shift is small and is not seen in the subsequent mergers in the sequence. We attribute the differ-

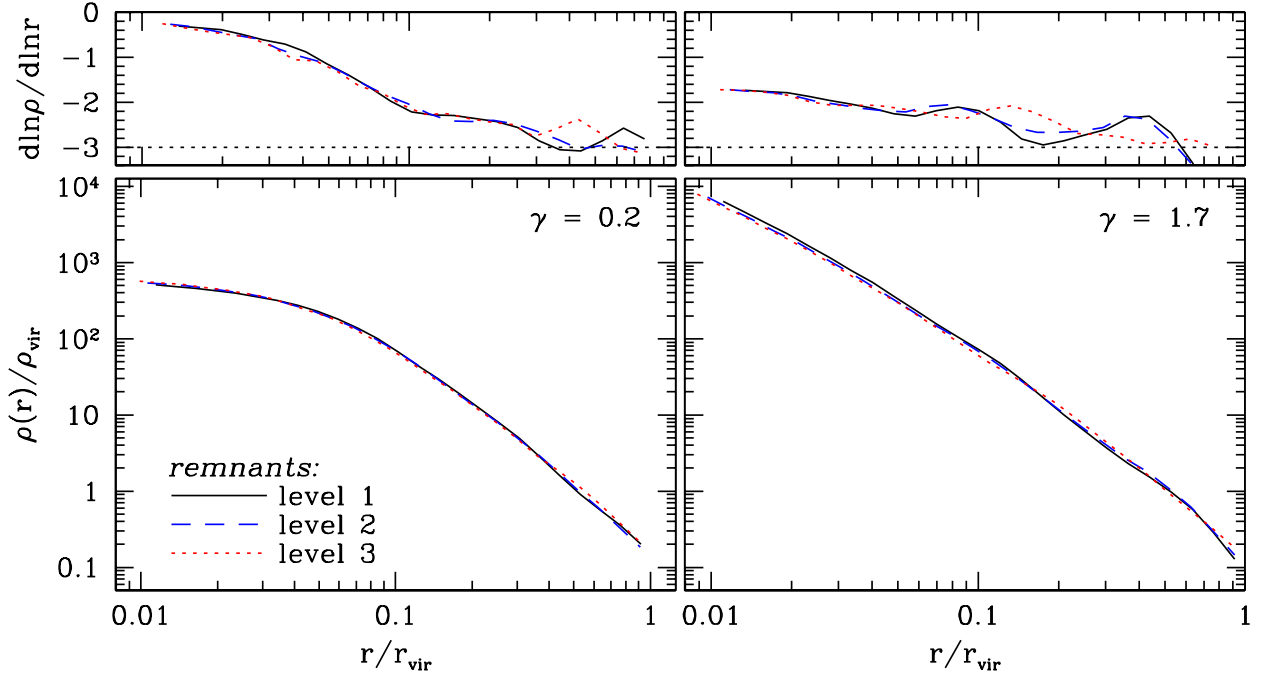


FIG. 7.— Density and logarithmic slope profiles as in Figure 3, but for the *sequence* of binary, parabolic mergers between identical halos. Each merger remnant was used as a progenitor in the next level of mergers after removing all unbound particles and randomly orienting its axis. The asymptotic density slope of the initial profiles is indicated in the *upper right-hand corner* of the bottom panels and remnant profiles are normalized to their own virial radii. The profiles from each level of the hierarchy are shown with different line type as indicated in the *lower left-hand corner*. Hierarchical merging does not serve to modify the inner slope and overall density profile shape down to the limit of our force resolution.

ence in the behavior between the initial model and level one merger remnant to the fact that the initial merger involves spherically-symmetric systems, while the higher level mergers are between triaxial halos.

Furthermore, it is worth pointing out the presence of wave-like features in the density profiles at $r \gtrsim 0.2r_{\text{vir}}$. These features are apparent in Figure 8 as we plot a quantity that emphasizes the details of the profiles, though they are also noticeable in Figs. 3, 5, and 7. They are associated with “shells” of particles left over after the merger and do not disappear even after several billion years of evolution subsequent to the completion of the collision. Therefore, even though the mergers involve smooth, structureless halos, the density profiles of the remnants are not completely smooth.

The last of the DM halo-only merger experiments that we explored involved the simultaneous collision of four identical halos. We performed these multiple merger experiments for shallow and steep initial profiles on both parabolic and radial initial orbits as described in detail in § 2.3. One might anticipate that in such simultaneous multiple mergers potential fluctuations are stronger and more violent, which may lead to a larger degree of relaxation compared to the binary mergers. The resulting profiles of $\rho(r)$ and $d \ln \rho(r) / d \ln r$ are shown in Figure 9. In this case, again, the merger remnants reflect the inner power-law indices and overall profile shapes of their progenitors and exhibit, at most, only a small shift in their scale radii relative to their virial radii. This rein-

forces our basic result, that the density structures of the merger remnants are nearly the same as their progenitors. This result cannot be circumvented by appealing to a complex merger hierarchy or episodes of multiple, nearly simultaneous, equal-mass mergers. In all cases, the final systems exhibit a remarkable memory of the density structure of their progenitors.

3.3. Galaxy Mergers

One of the goals of this study is to assess the general applicability and robustness of our results and the results of previous studies regarding the evolution of density profiles during dissipationless equal-mass mergers. As a further investigation of the generality of our primary findings, we perform numerical simulations of binary mergers between identical disk and elliptical galaxies constructed to resemble present-day systems. The models we adopt do not include gaseous dissipation, but include the various dissipationless components thought to dominate the mass distribution of real galaxies as well as adiabatic contraction of the DM halo during galaxy formation. These additional features allow orbital energy to be dissipated more quickly, the merger to come to completion significantly sooner, and the merger remnants to have different shapes with respect to the DM halo-only mergers (Kazantzidis et al. 2004a).

In the disk galaxy mergers, two identical spirals with self-gravitating disks, rotating DM halos and optional compact bulges merge in a variety of initial orbital configurations and relative orientations of the stellar disks.

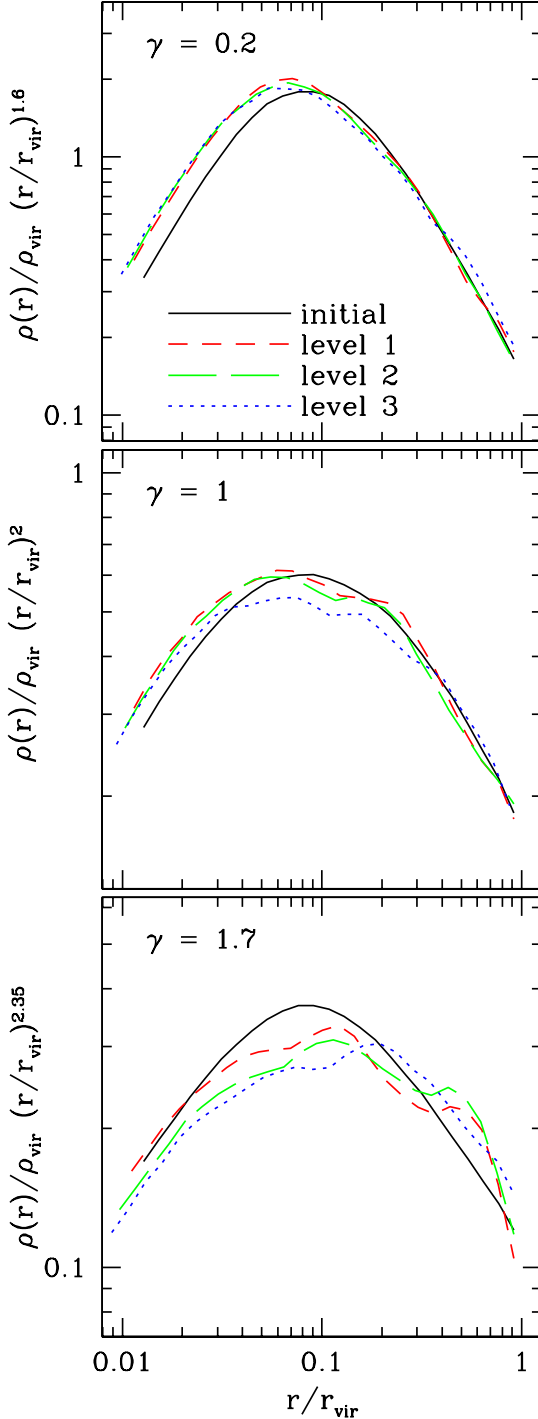


FIG. 8.— Density profile shapes, scale radii, and concentrations of the remnants in the sequence of binary mergers. The central density slopes of the initial profiles are indicated in the *upper left corners* of each panel. In order to emphasize the details of the profiles and the scale radius of the transition between the inner and outer power laws, we plot the product $\rho(r)r^{(\beta+\gamma)/2}$ on the vertical axis rather than $\rho(r)$. In each case, the remnant profiles are normalized to their own r_{vir} as defined in § 2.1. Under the assumption that each remnant can be described by the same set of $[\alpha, \beta, \gamma]$ slopes as the initial models, which seems well justified in this case, the maximum of the product $\rho(r)r^{(\beta+\gamma)/2}$ indicates the scale radius of the system.

In the elliptical galaxy mergers, two identical elliptical

galaxies with non-rotating DM halos and spherical stellar distributions collide on a parabolic orbit. Figure 10 displays results for all galaxy mergers performed in this study. In the left panels of Figure 10, we show the density and logarithmic slope profiles of DM in the halo+disk mergers with no stellar bulge component. The results concerning all other galaxy merger simulations are presented in the right panel of Figure 10.

The central density slopes and the overall density profile shapes of DM are maintained in mergers between identical systems consisting of multiple collisionless components. Hence, the presence of cold baryonic components does not render the chief result of this inquiry, that dissipationless mergers result in remnants that are practically scaled versions of their progenitors, ineffectual. Boylan-Kolchin et al. (2005) reached a similar conclusion in dissipationless mergers of elliptical galaxies for several different orbital configurations and mass models. The overall significance of our findings lies in the fact that the mixing of the various collisionless components during the mergers occurs in a manner that preserves the overall density structure of the DM component.

4. DISCUSSION

The results presented in this paper have interesting implications for the formation of a universal density profile in cosmological N -body simulations. We have established that the characteristic power-law indices of halos are not affected by major mergers, which should be ubiquitous during the early rapid-mass-accretion stages of halo evolution. Instead, this universal profile shape must be something that is imprinted on halos at the time of the collapse of the first gravitationally-bound objects. In hierarchical cosmological models, the amount of power in the initial spectrum of density perturbations is typically washed out on scales smaller than some critical scale. For example, in the popular case of the lightest supersymmetric particle this scale is set by the kinetic energies of the DM particles when they kinetically decouple from the thermal fluid (e.g., Chen et al. 2001; Hoffmann et al. 2001). Thus, there exists a typical “smallest” mass for collapsed structures, which is of order of $\sim 10^{-7}\text{--}10^{-5} M_{\odot}$ for the most frequently studied model of supersymmetric neutralino DM. The results reported in this paper can be used to argue that these first smallest structures must already have density profiles that follow an NFW-like universal form. This conclusion is in agreement with findings of direct numerical simulations. For example, Huss et al. (1999) and Shapiro et al. (2004) find that gravitational collapse leads to NFW-like profiles for a wide variety of initial conditions, while M99 and Diemand et al. (2005) show that in cosmological N -body simulations of the first virialized objects with masses near truncation mass of the power spectrum, these early halos have NFW-like density profiles.

Given that dissipationless late-time major mergers do not modify the shape of the profile, the problem of understanding the universality of the NFW-like density distribution can be relegated to understanding the reason why initial, rapid gravitational collapse leads to a density structure that is close to NFW. However, this is likely to be only an approximate picture. The actual mass assembly involves minor mergers, for which the density profile of the remnant will be a non-trivial average of the pro-

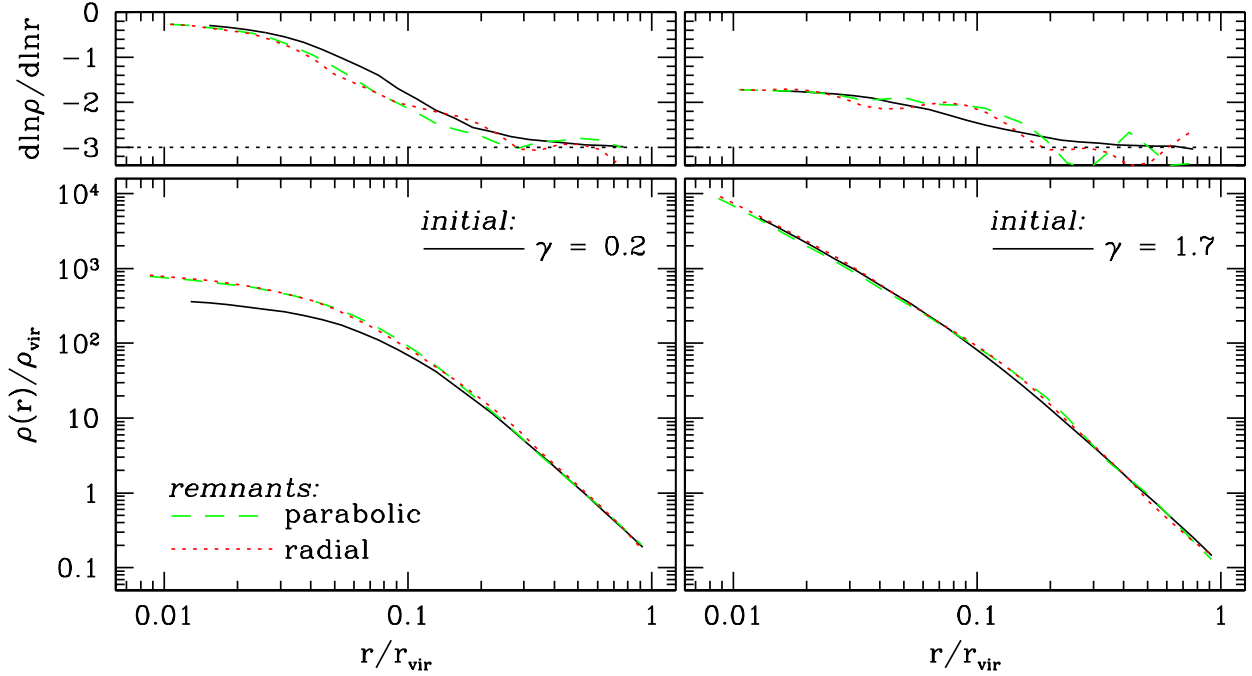


FIG. 9.— Density and logarithmic slope profiles as in Figure 3, but for the *quadruple* mergers between identical halos. The *left-hand panels* show results for the shallow initial density profiles while the *right-hand panels* show results for the steep initial density profiles. We plot results for both the parabolic (dashed lines) and radial (dotted lines) initial orbital configurations.

files of the progenitors, as smaller halos sink into the center and modify the inner density distribution (e.g., Syer & White 1998; Dekel et al. 2003; Ma & Boylan-Kolchin 2004). Therefore, it may be expected that the details of merger histories will induce some evolution of profile shape (e.g., Gao et al. 2005), which may explain the existence of significant scatter in the inner density profiles of cosmological structures (Tasitsiomi et al. 2004). Nevertheless, in the early rapid-accretion stage of halo evolution, the fraction of mass contributed by minor mergers should be relatively small and the bulk of the mass should be assembled via major mergers (e.g., Lacey & Cole 1993, 1994; Zentner & Bullock 2003) so the above conclusion can still be applicable.

In the context of the scaling relations of DM halos in cosmological N -body simulations, another intriguing result is reported in Figure 8. This plot illustrates that halo concentrations remain approximately constant through a sequence of mergers between identical systems. The controlled simulations we presented do not include the constant redefinition of the virial radii of *individual systems* that is due to the dilution of the mean background density with redshift. This dilution leads to a definition of virial radius that grows as $r_{\text{vir}}(a) \propto a$, where a denotes the scale factor. Combining this growth of virial radii with our measurement of the constancy of c , leads to a scaling of concentration as $c \propto r_{\text{vir}}(a)/r_s \propto a$ during cosmological evolution. This scaling is in broad agreement with the findings of the redshift evolution of halo concentrations in cosmological N -body simulations subsequent to an early phase of rapid-mass-accretion (e.g., Bullock et al. 2001b; Wechsler et al. 2002; Zhao et al.

2003; Tasitsiomi et al. 2004; Dolag et al. 2004). An interesting deviation from this is that Zhao et al. (2003) found that during the early rapid-mass-accretion period of halo growth, halo concentrations appear to remain approximately constant, suggesting qualitatively different behavior during the first stages of the collapse of rare density peaks.

We assessed the generality of our conclusions by initializing a sequence of parabolic encounters according to the conditions of cosmological mergers at redshift $z = 3$, rather than at $z = 0$. The initial systems followed the steep density profile and had the same M_{vir} as the standard halo models. We scaled the concentration parameter according to $c \propto (1+z)^{-1}$ for fixed mass objects (Bullock et al. 2001b; Wechsler et al. 2002; Zhao et al. 2003) and assumed that the first level of mergers initiates at $z = 3$. Our modeling results in a substantially denser initial system than before with $r_{\text{vir}} \simeq 79.5$ kpc, and correspondingly smaller orbital times. Indeed, the first level of the hierarchy concludes after only ~ 1.5 Gyr, as opposed to ~ 5 Gyr for the $z = 0$ case. The second and third level of mergers complete after ~ 1.8 Gyr and ~ 2.1 Gyr, respectively. The remnants at all levels of the high- z merger sequence retain excellent memories of the inner power-law indices and density profile shapes of their progenitors, in accord with the merger sequences of our fiducial simulations. Furthermore, the fraction of particles outside the virial radii of the remnants at each level is substantial (between ~ 30 and $\sim 50\%$), in agreement with the findings reported in § 3.2. As expected, the results of our study are insensitive to the overall densities and merger timescales that characterize

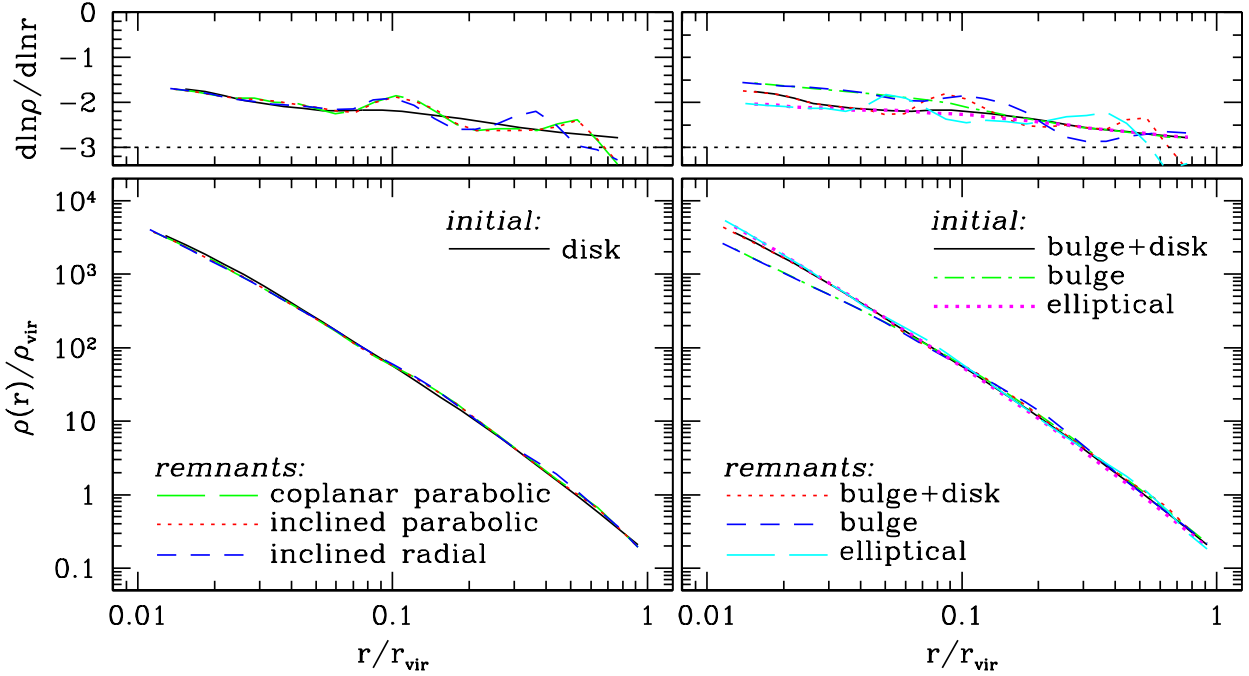


FIG. 10.— *Left:* Density and logarithmic slope profiles of DM as in Figure 3, but for the binary merger simulations between identical halo+disk *galaxy* models. The initial profile is shown by the solid line. Different line types correspond to various orbital configurations and relative disk inclinations as indicated in the lower left-hand corner of the bottom panel. *Right:* Profiles of DM in binary, parabolic merger simulations between identical multicomponent systems. Results are reported for systems consisting of a DM halo, a stellar disk, and a compact bulge, systems comprised of a DM halo and a bulge, and elliptical galaxies. The presence of cold baryonic components preserves the density structure of DM in mergers between identical systems.

mergers occurring at different cosmological epochs.

Recently, Lu et al. (2005) have argued that frequent major mergers associated with the rapid-mass-accretion phase may set the inner $\rho \propto r^{-1}$ profiles of CDM halos by effectively isotropizing the velocity field of DM particles during violent relaxation. Our simulations show that the shape of the density profile is well preserved during equal-mass mergers. Violent relaxation is therefore *incomplete*, as it does not erase memory of the progenitor properties. Further evidence to this is provided by numerical studies of mergers showing that the potential fluctuations necessary for violent relaxation are damped before the binding energies of particles are completely randomized (e.g., White 1978; Barnes 1992). We also observe that particle orbits in merger remnants, especially for the initial models with steep inner cusps, exhibit radial anisotropy at all radii. Although the initial progenitor models are fully isotropic (i.e., $\beta \equiv 1 - \sigma_t^2/2\sigma_r^2 = 0$ at all radii, where σ_t and σ_r are the tangential and radial velocity dispersion, respectively), merger remnants exhibit anisotropy that changes from mildly radial with $\beta \approx 0 - 0.2$ at small radii ($r/r_{\text{vir}} \lesssim 0.1$) to strongly radial with $\beta \approx 0.3 - 0.4$ on the outskirts. Such a radial dependence of β is rather similar to that observed in CDM halos formed in cosmological simulations (e.g., Cole & Lacey 1996; Colín et al. 2000; Faltenbacher et al. 2005). Therefore, equal-mass mergers do not lead to isotropic orbits. Nonetheless, we have probed the effect of mergers in the specific regime of equal-mass encounters that take place over several dy-

nical times. The situation may be qualitatively different when a large number of mergers, occurring in rapid succession, dramatically increase the depth of the potential over dynamical timescales, as assumed by Lu et al. (2005). Such rapid evolution of potential is likely to be relevant for the very earliest phases of collapse.

Our findings can be used to place constraints on the expectations for the DM distribution in galaxies and clusters. Loeb & Peebles (2003) and Gao et al. (2004) have put forward the hypothesis that one of the fundamental properties of the NFW density profile is that it is a dynamical attractor in collisionless evolution. More specifically, these authors argued that if the density structure of a collisionless system were to deviate from the NFW profile, perhaps due to baryonic dissipation or some other process, subsequent dissipationless major merging would drive the density distribution toward the NFW form. This “attractor” hypothesis, combined with observations that stars dominate gravitationally in the centers of galaxies, would imply shallower DM density profiles in the inner regions of clusters than predicted by collisionless cosmological simulations (e.g., Sand et al. 2002). However, the numerical results presented in this study do not support the attractor hypothesis. Our simulations show that the inner power-law indices and the overall shapes of density profiles remain unmodified during collisionless equal-mass binary mergers, even after a sequence of collisions, or in simultaneous multiple mergers. This conclusion persists even if the progenitor sys-

tems contain cold stellar components with a variety of properties.

An immediate consequence is that the effects of gas cooling and baryon condensation in halo centers, which steepen the inner DM density profiles, are maintained in subsequent dissipationless major merging. This is consistent with the results of Gnedin et al. (2004), who showed that the effects of cooling at high redshifts are retained in cosmological simulations to the present day and can be well described by the adiabatic contraction model, even when DM halos undergo a period of dissipationless evolution.

One of the many routes to forming bright elliptical galaxies in hierarchical cosmological models involves dissipationless merging in their late stages of evolution. Though the details of this picture have yet to come into focus, the results reported in this study are relevant to scenarios of elliptical galaxy formation. Observed bright and faint ellipticals exhibit a dichotomy in their inner stellar density distributions. Bright ellipticals tend to have flatter central stellar density profiles compared to faint ellipticals, which exhibit cuspy profiles (e.g., Faber et al. 1997; Kormendy 1999). Our findings intimate that dissipationless hierarchical merging of faint ellipticals alone cannot alone be invoked as a mechanism for forming bright elliptical galaxies. Any such scenario would require an additional process that should be responsible for the flattening of the inner density distributions. As an example, the prevalence of relatively low-density cores in bright elliptical galaxies may be a consequence of the existence of supermassive black holes and their interactions with the stellar backgrounds (Makino & Ebisuzaki 1996; Merritt & Cruz 2001).

An analytical framework exists that aids in the understanding of our numerical results. Undoubtedly, our dissipationless simulations must conform to Liouville's theorem demanding that the phase-space density of a dynamical system that undergoes collisionless evolution to a new state cannot increase. Nevertheless, as has also been emphasized by Boylan-Kolchin & Ma (2004), Liouville's theorem applies to a six-dimensional quantity and there is no *a priori* reason to expect that both configuration and momentum space distributions should be independently conserved. In general the distributions in these subspaces are *not* conserved. In fact, our simulations show that both configuration and momentum space distributions are altered during mergers.

More complicated treatment of phase-space evolution is needed to draw conclusions about evolution of density profiles (Mathur 1988; Dehnen 2005). In particular, Dehnen (2005) recently showed that for phase-space density f , the *excess mass function* $D(f)$, defined as the difference between the mass with phase-space density $> f$ and the product of f and the volume of phase-space with density $> f$, can only decrease upon mixing. This mixing theorem and the simple properties of $D(f)$ as $f \rightarrow \infty$ for self-gravitating density cusps can then be used to prove that a merger remnant cannot have a density cusp steeper than that of the steepest progenitor. Dehnen (2005) also argued that reducing the slope of the density cusp would require arbitrarily large dilution of the phase-space density so that it seems implausible that the remnant could have an inner cusp shallower than the steepest progenitor cusp.

Our findings are in agreement with the conclusions of Dehnen (2005). Indeed, Figure 3 illustrates that in a merger of two identical power-law density profiles, the remnant exhibits a power-law inner density slope equal to that of the progenitors. In addition, the results embodied by Figure 5 hint that in mergers between halos of very different inner density power laws, the remnant has a central density slope slightly shallower than that of the steepest of the progenitors on scales that are of practical concern for galaxies. However, the results of Dehnen (2005) apply asymptotically as $r \rightarrow 0$ and our simulations simply may not resolve sufficiently small radii for the asymptotic result to hold. In this regard, we see no evidence that the second conclusion of Dehnen (2005) is violated but higher-resolution numerical simulations of merging density cusps are required to test this conjecture more extensively.

Our findings also shed light on the resilience of density cusps to gravitational interactions. Kazantzidis et al. (2004c) elucidated the dynamical effect of tides on the central density profiles of cuspy satellite halos. These authors employed collisionless, high-resolution N -body cosmological simulations with simulations of the tidal stripping of individual satellites orbiting within a static host potential and showed that the density distribution retains its initial inner power-law index as the satellite experiences mass loss. Their analysis revealed that the central density cusp is notably stable to tidal shocks and gravitational stripping. The results reported in this paper combined with those of Kazantzidis et al. (2004c), suggest that density cusps, once formed, are extremely difficult to disrupt or even to modify in any significant way.

The preservation of the inner power laws of halo density profiles has intriguing implications for tests of the nature of DM through observations of galactic and subgalactic structure. In alternatives to CDM models such as WDM (e.g., Pagels & Primack 1982; Colombi et al. 1996; Hogan & Dalcanton 2000) or DDM (e.g., Kaplinghat 2005; Cembranos et al. 2005) the DM particles typically have non-negligible momenta which leads to a suppression of small-scale structure for two reasons. The first reason is that the power spectrum of density fluctuations on small scales is damped by the free-streaming of the particles (e.g., Ma 1996; Bode et al. 2001; Kaplinghat 2005). The second reason is that these particles are restricted to finite phase-space densities (Tremaine & Gunn 1979; Hogan & Dalcanton 2000; Kaplinghat 2005). The phase-space constraint is thought to induce a cored inner profile of nearly constant density in small and early-forming DM halos, because the very high phase-space densities of cusp-like profiles are unachievable (e.g., Avila-Reese et al. 2001). The findings of the present study imply that if the small, early-forming building blocks of larger halos were formed with cored density profiles, these cores should be well-preserved during the hierarchical assembly of larger halos, in the very least during periods of rapid major mergers. The signatures of the alternative DM could, therefore, be possibly observed in accurate measurements of the rotation curves of DM-dominated galaxies at small scales (e.g., de Blok et al. 2001; Salucci et al. 2003; Weldrake et al. 2003; Simon et al. 2005) or the flux anomalies in strong-lens systems (e.g., Dalal & Kochanek 2002; Zentner & Bullock 2003;

Rozo et al. 2005). This could potentially provide fundamental constraints on the properties of the DM particles.

We conclude by emphasizing that in this article, we have only addressed the evolution of density profiles in mergers between equal-mass systems. Recent works have examined more general situations involving systems with a spectrum of masses and reached similar conclusions (Boylan-Kolchin & Ma 2004; Aceves & Velazquez 2005). This fact allows us to argue that our main findings can be generalized to all unequal-mass *major* mergers with some degree of confidence.

In our modeling, we have also implicitly assumed that cuspy halos have a higher phase-space density in the inner regions than cored profiles. The fact that in hybrid mergers the inner density slope of the remnant is closer to that of the steepest of the progenitors suggests that the quantity that drives the evolution of the profile is the phase-space density. However, it is not difficult to imagine merging scenarios where this situation can be reversed as, for example, in cases of unequal-mass mergers or encounters between systems with considerably different concentration parameters. We defer a detailed numerical study of these considerations to future work.

5. SUMMARY

Using a large suite of controlled, dissipationless N -body simulations we have explored the evolution of DM density profiles in equal-mass mergers of DM halos and multicomponent galaxies. A common feature of the majority of previous related investigations is that they did not consider the effect of hierarchical merging that characterizes CDM models, nor did they examine the role of baryonic components on the density structure of merger remnants. In contrast, our numerical experiments are performed in degrees of increasing complexity. We present an ensemble of simulations comprised not only of binary encounters, but also sequences of mergers and collisions between multiple progenitors in order to study the range of behaviors that are realized in the context of cosmological structure formation. We have also probed a wider range of parameter space with respect to earlier studies by varying the initial orbital configurations and orbital energies in an effort to establish the generality of our main results. Finally, we examined collisions between systems with multiple components consisting of rotating DM halos, stellar disks, and stellar spheroids. This enabled us to elucidate the impact of internal angular momentum and the presence of cold baryons on our findings. We find that the merger remnants in our simulations conform to a set of several simple and general results that can be summarized as follows.

1. Binary mergers between identical DM halos with density structures described by various asymptotic power-law indices $\rho \propto r^{-\gamma}$ ranging from steep cusps to core-like profiles produce remnants with inner density slopes equal to those of the progenitors. Furthermore, the overall shape of the remnant density distribution constitutes a remarkable reflection of that of the initial systems. If the progenitor halos are constructed with appreciably different asymptotic power-law indices, the inner density slope of the remnant is closer to that of the steepest of the initial systems. These conclusions hold for a wide

range of orbital energies.

2. The aforementioned findings remain valid for a variety of encounter configurations including sequences of several consecutive merger events, designed to mimic hierarchical merging, and simultaneous collisions of several systems. Overall, the inner slopes and shapes of density profiles are remarkably robust during dissipationless evolution, regardless of the number of mergers and initial conditions associated with the encounters. Dissipationless equal-mass mergers do not provide a mechanism for driving the density profiles of collisionless matter toward a universal form, contradicting the hypothesis that the NFW profile behaves as a dynamical attractor (Loeb & Peebles 2003; Gao et al. 2004).
3. In binary mergers between identical systems, particles from both systems contribute equally to the final density profile at all radii, as must be the case due to symmetry. In mergers between systems of markedly different inner density power laws, the central regions of the remnants are dominated by particles originating from the system with the steeper inner density slope. The steepest inner core survives, almost unaffected, in the remnant.
4. Remnants in mergers between equal-mass systems contain significant fractions of their bound mass, $\sim 25 - 50\%$, well beyond their formal virial radii and extending out to $\approx 2 - 4r_{\text{vir}}$. This suggests that the virial mass is not simply additive in mergers, as is commonly assumed in many semi-analytic models of halo and galaxy evolution. Semi-analytic models may significantly overestimate the mass and density within the virial radii of merger remnants.
5. Mergers between identical DM halos produce self-similar remnants in the sense that their scale radii, r_s , defined as the radii at which the density profiles transition from an inner to an outer power law, are very similar to those of the progenitors when measured in units of the halo virial radii, r_{vir} . In other words, halo concentrations remain essentially unmodified during equal-mass encounters and the remnants correspond to scaled versions of their progenitors.
6. Mergers between identical systems containing cold stellar components in the form of disks, spheroids, or a combination of the two, in addition to the extended DM halos, exhibit a degree of self-similarity akin to those of the DM halo-only mergers. Namely, the overall shape of the density profiles and the inner density slopes of DM are maintained in the remnants. Particle mixing preserves the density structure of the DM component. The effects of gaseous dissipation on the DM profiles of the progenitor systems will be retained in the density distribution of their descendants under dissipationless major merging.

The authors acknowledge many stimulating discussions with Tom Abel, Michael Boylan-Kolchin, Vincent Eke, Oleg Gnedin, Anatoly Klypin, Abraham Loeb, John Magorrian, Lucio Mayer, David Merritt, Houjun Mo, Daisuke Nagai, Robert Sakamano, Joachim Stadel, and Risa Wechsler. SK is supported by the Swiss National Science Foundation and by The Kavli Institute for Cosmological Physics (KICP) at The University of Chicago. ARZ is funded by the KICP and the National Science

Foundation (NSF) under grant No. NSF PHY 0114422. AVK is supported by the NSF under grants No. AST-0206216 and AST-0239759, by NASA through grant NAG5-13274, and by the KICP. The numerical simulations used in this study were performed on the zBox supercomputer at The University of Zürich and on the Intel cluster at the Cineca Supercomputing Center in Bologna. This research made use of the NASA Astrophysics Data System.

REFERENCES

Aceves, H. & Velazquez, H. 2005, RevMexAA submitted (astro-ph/0506290)

Ascasibar, Y., Yepes, G., Gottlöber, S., & Müller, V. 2004, MNRAS, 352, 1109

Avila-Reese, V., Colín, P., Valenzuela, O., D'Onghia, E., & Firmani, C. 2001, ApJ, 559, 516

Avila-Reese, V., Firmani, C., Klypin, A., & Kravtsov, A. V. 1999, MNRAS, 310, 527

Barnes, J. & White, S. D. M. 1984, MNRAS, 211, 753

Barnes, J. E. 1992, ApJ, 393, 484

Barnes, J. E. 1999, in IAU Symp. 186: Galaxy Interactions at Low and High Redshift, 137

Barnes, J. E. & Hernquist, L. 1996, ApJ, 471, 115

Benson, A. J. 2005, MNRAS, 358, 551

Benson, A. J., Frenk, C. S., Baugh, C. M., Cole, S., & Lacey, C. G. 2003, MNRAS, 343, 679

Blumenthal, G. R., Faber, S. M., Flores, R., & Primack, J. R. 1986, ApJ, 301, 27

Blumenthal, G. R., Faber, S. M., Primack, J. R., & Rees, M. J. 1984, Nature, 311, 517

Bode, P., Ostriker, J. P., & Turok, N. 2001, ApJ, 556, 93

Boylan-Kolchin, M. & Ma, C. 2004, MNRAS, 349, 1117

Boylan-Kolchin, M., Ma, C.-P., & Quataert, E. 2005, MNRAS, 362, 184

Bullock, J. S., Dekel, A., Kolatt, T. S., Kravtsov, A. V., Klypin, A. A., Porciani, C., & Primack, J. R. 2001a, ApJ, 555, 240

Bullock, J. S., et al. 2001b, MNRAS, 321, 559

Cembranos, J. A. R., Feng, J. L., Rajaraman, A., & Takayama, F. 2005, PRD submitted (hep-ph/0507150)

Chen, X., Kamionkowski, M., & Zhang, X. 2001, Phys. Rev. D, 64, 021302

Cole, S. & Lacey, C. 1996, MNRAS, 281, 716

Colín, P., Avila-Reese, V., & Valenzuela, O. 2000, ApJ, 542, 622

Colombi, S., Dodelson, S., & Widrow, L. M. 1996, ApJ, 458, 1

Dalal, N. & Kochanek, C. S. 2002, ApJ, 572, 25

de Blok, W. J. G., McGaugh, S. S., & Rubin, V. C. 2001, AJ, 122, 2396

Dehnen, W. 2005, MNRAS, 360, 892

Dekel, A., Arad, I., Devor, J., & Birnboim, Y. 2003, ApJ, 588, 680

Diemand, J., Moore, B., & Stadel, J. 2004, MNRAS, 353, 624

—. 2005, Nature, 433, 389

Dolag, K., Bartelmann, M., Perrotta, F., Baccigalupi, C., Moscardini, L., Meneghetti, M., & Tormen, G. 2004, A&A, 416, 853

Dubinski, J. & Carlberg, R. G. 1991, ApJ, 378, 496

Eddington, A. S. 1916, MNRAS, 76, 572

Eke, V. R., Navarro, J. F., & Frenk, C. S. 1998, ApJ, 503, 569

Eke, V. R., Navarro, J. F., & Steinmetz, M. 2001, ApJ, 554, 114

Faber, S. M., et al. 1997, AJ, 114, 1771

Faltenbacher, A., Kravtsov, A. V., Nagai, D., & Gottlöber, S. 2005, MNRAS, 358, 139

Farouki, R. T., Shapiro, S. L., & Duncan, M. J. 1983, ApJ, 265, 597

Fukushige, T., Kawai, A., & Makino, J. 2004, ApJ, 606, 625

Fukushige, T. & Makino, J. 1997, ApJ, 477, L9+

—. 2001, ApJ, 557, 533

Fulton, E. & Barnes, J. E. 2001, Ap&SS, 276, 851

Gao, L., Loeb, A., Peebles, P. J. E., White, S. D. M., & Jenkins, A. 2004, ApJ, 614, 17

Gao, L., White, S. D. M., Jenkins, A., Frenk, C. S., & Springel, V. 2005, MNRAS, 853

Ghigna, S., Moore, B., Governato, F., Lake, G., Quinn, T., & Stadel, J. 1998, MNRAS, 300, 146

Gnedin, O. Y., Kravtsov, A. V., Klypin, A. A., & Nagai, D. 2004, ApJ, 616, 16

Graham, A. W., Merritt, D., Moore, B., Diemand, J., & Terzic, B. 2005, AJ submitted (astro-ph/509417)

Hernquist, L. 1990, ApJ, 356, 359

—. 1993, ApJS, 86, 389

Hofmann, S., Schwarz, D. J., & Stöcker, H. 2001, Phys. Rev. D, 64, 083507

Hogan, C. J. & Dalcanton, J. J. 2000, PRD, 62, 063511

Huss, A., Jain, B., & Steinmetz, M. 1999, ApJ, 517, 64

Kaplinghat, M. 2005, PRD submitted (astro-ph/0507300)

Kazantzidis, S., Kravtsov, A. V., Zentner, A. R., Allgood, B., Nagai, D., & Moore, B. 2004a, ApJ, 611, L73

Kazantzidis, S., Magorrian, J., & Moore, B. 2004b, ApJ, 601, 37

Kazantzidis, S., Mayer, L., Mastropietro, C., Diemand, J., Stadel, J., & Moore, B. 2004c, ApJ, 608, 663

Kazantzidis, S., et al. 2005, ApJ, 623, L67

Khochfar, S. & Burkert, A. 2005, A&A accepted (astro-ph/0309611)

Klypin, A., Kravtsov, A. V., Bullock, J. S., & Primack, J. R. 2001, ApJ, 554, 903

Klypin, A., Zhao, H., & Somerville, R. S. 2002, ApJ, 573, 597

Knebe, A., Devriendt, J. E. G., Mahmood, A., & Silk, J. 2002, MNRAS, 329, 813

Kormendy, J. 1999, in ASP Conf. Ser. 182: Galaxy Dynamics - A Rutgers Symposium, 124

Kravtsov, A. V., Klypin, A. A., Bullock, J. S., & Primack, J. R. 1998, ApJ, 502, 48

Lacey, C. & Cole, S. 1993, MNRAS, 262, 627

—. 1994, MNRAS, 271, 676

Loeb, A. & Peebles, P. J. E. 2003, ApJ, 589, 29

Lu, Y., Mo, H. J., Katz, N., & Weinberg, M. D. 2005, MNRAS submitted (astro-ph/0508624)

Ma, C.-P. 1996, ApJ, 471, 13

Ma, C.-P. & Boylan-Kolchin, M. 2004, Physical Review Letters, 93, 021301

Makino, J. & Ebisuzaki, T. 1996, ApJ, 465, 527

Mathur, S. D. 1988, MNRAS, 231, 367

Merritt, D. & Cruz, F. 2001, ApJ, 551, L41

Merritt, D., Navarro, J. F., Ludlow, A., & Jenkins, A. 2005, ApJ, 624, L85

Mo, H. J., Mao, S., & White, S. D. M. 1998, MNRAS, 295, 319

Moore, B., Kazantzidis, S., Diemand, J., & Stadel, J. 2004, MNRAS, 354, 522

Moore, B., Quinn, T., Governato, F., Stadel, J., & Lake, G. 1999, MNRAS, 310, 1147

Navarro, J. F., Frenk, C. S., & White, S. D. M. 1996, ApJ, 462, 563 (NFW)

—. 1997, ApJ, 490, 493

Navarro, J. F., et al. 2004, MNRAS, 349, 1039

Pagels, H. & Primack, J. R. 1982, Physical Review Letters, 48, 223

Power, C., et al. 2003, MNRAS, 338, 14

Prada, F., Klypin, A. A., Simonneau, E., Betancort-Rijo, J., Patiri, S., Gottlöber, S., & Sanchez-Conde, M. A. 2005, ApJ submitted (astro-ph/0506432)

Reed, D., et al. 2005, MNRAS, 357, 82

Rozo, E., Zentner, A. R., Bertone, G. F., & Chen, J. 2005, ApJ submitted, (astro-ph/0506573)

Ryden, B. S. & Gunn, J. E. 1987, ApJ, 318, 15

Salucci, P., Walter, F., & Borriello, A. 2003, A&A, 409, 53

Sand, D. J., Treu, T., & Ellis, R. S. 2002, ApJ, 574, L129

Shapiro, P. R., Iliev, I. T., Martel, H., Ahn, K., & Alvarez, M. A. 2004, Progress in Dark Matter Research, submitted (astro-ph/0409173)

Shen, S., et al. 2003, MNRAS, 343, 978

Simon, J. D., Bolatto, A. D., Leroy, A., Blitz, L., & Gates, E. L. 2005, ApJ, 621, 757

Somerville, R. S. & Primack, J. R. 1999, MNRAS, 310, 1087

Spergel, D. N., et al. 2003, ApJS, 148, 175

Springel, V., Di Matteo, T., & Hernquist, L. 2005, MNRAS, 361, 776

Springel, V. & White, S. D. M. 1999, MNRAS, 307, 162

Stadel, J. G. 2001, Ph.D. Thesis, Univ. of Washington

Stoehr, F., White, S. D. M., Tormen, G., & Springel, V. 2002, MNRAS, 335, L84

Syer, D. & White, S. D. M. 1998, MNRAS, 293, 337

Taffoni, G., Mayer, L., Colpi, M., & Governato, F. 2003, MNRAS, 341, 434

Tasitsiomi, A., Kravtsov, A. V., Gottlöber, S., & Klypin, A. A. 2004, ApJ, 607, 125

Taylor, J. E. & Babul, A. 2004, MNRAS, 348, 811

Tremaine, S. & Gunn, J. E. 1979, PRL, 42, 407

Villumsen, J. V. 1983, MNRAS, 204, 219

Wechsler, R. H., Bullock, J. S., Primack, J. R., Kravtsov, A. V., & Dekel, A. 2002, ApJ, 568, 52

Weldrake, D. T. W., de Blok, W. J. G., & Walter, F. 2003, MNRAS, 340, 12

White, S. D. M. 1978, MNRAS, 184, 185

White, S. D. M. & Rees, M. J. 1978, MNRAS, 183, 341

Zeldovich, Y. B., Klypin, A. A., Khlopov, M. Y., & Chechetkin, V. M. 1980, Soviet J. Nucl. Phys., 31, 664

Zentner, A. R. & Bullock, J. S. 2003, ApJ, 598, 49

Zentner, A. R., Berlind, A. A., Bullock, J. S., Kravtsov, A. V., & Wechsler, R. H. 2005, ApJ, 624, 505

Zhao, D. H., Mo, H. J., Jing, Y. P., & Börner, G. 2003, MNRAS, 339, 12

Zhao, H. 1996, MNRAS, 278, 488